Republic of Iraq
Ministry of Higher Education
and Scientific Research
University of Babylon
College of Materials Engineering
Department of Ceramic and Building Materials

Studying the Mechanical Properties of Alumina-Magnesia Ceramics Using Digital Image Correlation (DIC) and Optimization Methods

A Thesis
Submitted to the Council of the College of Materials Engineering / University of Babylon in Partial Fulfillment of the Requirements for the Master degree in Materials Engineering / Ceramics

By
Ehab Ahmed Obaid Abdel Reda

(B.Sc. In Materials Engineering)
(2008)
(High Diploma in Ceramics and Building Materials Engineering)
(2018)

Supervised by

Prof.
Dr. Mohsin Abbas Aswad

Prof.
Dr. Mohammed A. Ahmed Al-Dujaili

2023 A.C

1444 A.H

بسم الله الرحمن الرحيم

اقرأ باسمِ ربِّكَ الَّذي خَلَق ﴿1﴾ خَلَقَ الإنسانَ من عَلَق
﴿2﴾ اقرأ وربُّكَ الأكرم ﴿3﴾ الَّذي علَّمَ بالقَلَم ﴿4﴾ علَّم
الإنسانَ ما لم يعلم ﴿5﴾

صدق الله العلي العظيم

الآية ﴿1-5﴾ من سورة العلق

The Certificate of supervisors

We certify that this thesis entitled " ***Studying the Mechanical Properties of Alumina-Magnesia Ceramics Using Digital Image Correlation and Optimization Methods*** " is Prepared by (***Ehab Ahmed Obaid Alramahi***) under our supervision at the Department of Ceramics and Building Materials / College of Materials Engineering / University of Babylon in partial fulfillment of the requirements for the degree of Master in Ceramics and Building Materials.

Signature :
Name : Prof. Dr. Mohsin Abbas Aswad
(supervisor)
Date : / / 2023

Signature :
Name : Prof. Dr. Mohammed A. Ahmed Al-dujaili
(supervisor)
Date : / / 2023

In view of the available recommendations. I forward this thesis for debate by the examination committee.

Signature:
Prof. Dr. Mohsin Abbas Aswad
Date:
Head of Ceramics and Building Materials

Dedication

To my father's pure soul, who planted in my heart love of science and learning and always pushed me forward.
To All My Family.

Ehab Alramahi
2023

Acknowledgments

First of all, all thanks be for ***ALLAH*** Lord of all creations who enable me to achieve this work.

I would like to express my gratitude to my supervisors, ***Dr. Mohsin Abbas Aswad*** and ***Dr. Mohammed A. Ahmed Al-Dujaili***, for their guidance, advice and enthusiastic encouragement throughout this investigation.

I am very grateful to my family especially my father, mother, and my sincere wife and my daughters for their assistance, encouragement and support during the period of preparing this work.

Special thanks to the faculty staff members of the Ceramic Department.

My deep appreciation goes to the members of Ceramic materials laboratories especially **Eng.Basseem, Eng.Ibtisam, Eng.Rehab, Eng.Khansaa** and all the engineers in the liberatory.

I would also like to thank ***everyone*** helping me in my work from the beginning until finish.

Ehab Alramahi

2023

Abstract

This work shows the importance of Alumina in the many applications. The object of the study is to preparing alumina mixed with different percentage of magnesia (2, 4, 6, 8, 10) wt%, for its high performance and low price, and studying the effect of the magnesia percentage on the properties of the products and possibility of (Al_2MgO_4) spinal production and the effect of the spinal on the properties. The preparing powder and resulting products were characterized by X-ray diffraction, particle size, bulk density, SEM observation, hardness, and fracture toughness, and using an image correlation technique, and make an optimization model for the process conditions and results.

Alumina powder with particle sizes 4.7μm that used in the sample preparation of ceramic specimen. The alumina was milled with (2,4,6,8,10) wt% magnesia 4.2μm powder separately by ball milling for 4 hours. Dense samples were produced by uniaxially pressing under 200 MPa using stainless steel die. The samples were then dried for 6 hours in 150ºC and left for 24 hours under room temperature and presureless sintering were conducted at 1300ºC & 1400ºC for 4 hours at heating rate 10 ºC/min in the programmable furnace.

The results showed that the critical load for initiation the crack for Alumina mixed with (0, 2, 4, 6, 8, 10 wt.%) Magnesia was (7, 9, 12, 6, 7, 8) N respectively, and the fracture toughness was (0.713, 0.857, 1.264, 0.648, 0.831) MPa. $\sqrt{m}$ respectively.

The tests conducted on the samples were shown that the percentage of 4% wt% MgO gave the best mechanical properties compared to the rest of the percentages.

The results of DIC showed that by adding MgO, the resistance to the crack propagation would increase and the crack take longer time to cause failure, gave a localized strain map for every specimen, and measured the COD precisely.

Using an optimization model to get an optimum production condition by analytical method was a useful method when have a numerous production and results variables.

Table of Contents

List of Figures

List of Tables

Symbols and Abbreviations

Abbreviation or Symbol	Description
Al_2O_3	*Alumina*
MgO	*Magnesia*
ASTM	*American Society for Testing Materials*
E	*Young's Modules*
v	*Poisson's ratio*
DIC	*Digital Image Correlation*
COD	*Crack Opening displacement*
CMOD	*Crack Mouth Opening displacement*
CTOD	*Crack Tip Opening displacement*
KIC	*Fracture Toughness*
HV	*Vickers' microhardness*
R-curve	*Resistance curve*
P.S	*Particle Size*
et al	*Others*
SEM	*Scanning Electron Microscope*
XRD	*X-Ray Diffraction*
PVA	*Polyvinyl Alcohol*
SENB	*single edge notched beam*
SEVNB	*single edge V-notched beam*
CNB	*chevron notch beam*
DOE	*Design of experiments*
ZTA	*Zirconia Toughened Alumina*
HA	*hydroxyapatite*
ROI	*Region of interesting*

جمهورية العراق
وزارة التعليم العالي والبحث العلمي
جامعة بابل
كلية هندسة المواد
قسـم هندسة السيراميك ومواد البناء

دراسة الخواص الميكانيكية لمادة ألومينا-مغنيسيا بإستخدام الارتباط الرقمي وطرق الأمثلية

رسالة

مقدمة الى قسم السيراميك ومواد البناء في كلية هندسة المواد / جامعة بابل وهي

جزء من متطلبات نيل درجة الماجستير في هندسة المواد / السيراميك

من قبل
إيهاب احمد عبيد عبد الرضا
بكالوريوس هندسة مواد
(2008)
دبلوم عالي هندسة سيراميك ومواد بناء
(2018)

بإشراف

أ. د.
محسن عباس اسود

أ. د.
محمد عاصي الدجيلي

2023 م

1444 هـ

الخلاصة

توضح هذه الأطروحة أهمية الألومينا في العديد من التطبيقات. الهدف من الدراسة هو تحضير الألومينا مشوبة بنسبة وزنية مختلفة من المغنيسيا (0، 2، 4، 6، 8، 10) ٪، بسبب أدائها العالي وتوافقها الحيوي العالي وسعرها المنخفض، ودراسة تأثير نسبة المغنيسيا على خصائص المنتجات وإمكانية إنتاج (Al_2MgO_4) وتأثيره على الخصائص للمادة الناتجة. تم توصيف مسحوق التحضير والمنتجات الناتجة عنه بحيود الأشعة السينية ، وحساب حجم الجسيمات ، والكثافة الظاهرية ، وفحص البنية المجهرية بواسطة SEM ، وفحص الصلادة ، وحساب متانة الكسر بطرق عملية وباستخدام برنامج DIC، وعمل نموذج الأمثلية لظروف العملية ونتائجها.

مسحوق الألومينا المستخدم كان بحجم حبيبي 4.7 مايكرومتر والذي استخدم في إعداد العينة السيراميكية. تم خلط الألومينا مع (0،2،4،6،8،10) بالوزن ٪ مسحوق المغنيسيا 4.2 مايكرومتر بشكل منفصل باستخدام طاحونة الكرات لمدة 4 ساعات. تم إنتاج عينات كثيفة عن طريق الكبس المحوري بضغط 200 ميجا باسكال باستخدام قوالب الفولاذ المقاوم للصدأ. ثم تم تجفيف العينات لمدة 6 ساعات في 150 درجة مئوية وتركت لمدة 24 ساعة تحت درجة حرارة الغرفة وتم إجراء التلبيد عند 1300 درجة مئوية و 1400 درجة مئوية لمدة 4 ساعات بمعدل تسخين 10 درجات مئوية / دقيقة في الفرن القابل للبرمجة.

أظهرت النتائج لعينات الالومينا المخلوطة مع المغنيسيا بنسب وزنية (2, 4, 6, 8, 10 %) أن الحمل الحرج لنشوء الكسر كان (7, 9, 12, 6, 7, 8) نيوتن, تباعا وكانت متانة الكسر للعينات (0.713, 0.857, 1.264, 0.648, 0.699, 0.831) ميجا باسكال لكل متر, تباعا.

أظهرت الاختبارات التي أجريت على العينات أن النسبة المئوية 4٪ مغنيسيا أعطت أفضل الخواص الميكانيكية مقارنة بباقي النسب المئوية.

أظهرت نتائج الارتباط الصوري الرقمي (DIC) أنه بإضافة المغنيسيا ، ستزداد مقاومة تقدم الشق وسيستغرق الشق وقتًا أطول للتسبب في الفشل ، وأعطت خريطة إجهاد موضعية لكل عينة ، وقياس (COD) بدقة.

كان استخدام نموذج الامثلية للحصول لاعطاء حالة الإنتاج المثلى بالطريقة التحليلية طريقة مفيدة عندما يكون لديك العديد من متغيرات الإنتاج والنتائج.

Chapter One

Introduction

1.1 Introduction

Based on their unique features, such as excellent strength, high hardness, strong wear resistance, and chemical stability, advanced ceramic materials are used in numerous applications, including cutting inserts, electrical applications, and armor. In many applications, ceramics are often exposed to dynamic loading. The effectiveness of ceramics in various applications is primarily determined by how they react to dynamic loads. Unfortunately, the exact process governing how brittle materials like ceramics fracture when subjected to dynamic stress is yet unknown. This is because ceramics' mechanical reaction is more complicated than that of metals, especially when considering the effects of dynamic loading and multiaxial stress states[1].

The alumina may be viewed as a typical engineering ceramics representative. Particularly under harsh climatic circumstances, these qualities make them extremely desirable for structural applications such as automotive, aerospace, biomedical, and cutting tool products. As a result, ceramic - especially alumina - becomes the material most frequently used in applications requiring wear resistance, making it particularly significant due to its wide range of uses in areas such as chemical inertia, significant fracture toughness, relatively low cost, high hardness, high resistance to erosion, stability at high temperatures, elevated resistance electrical, and high availability[2].

One of the most critical and crucial steps in the fabrication of a ceramic component or structure is consolidation. To transform from a green body to a

rigid body, most ceramic components manufactured using powder metallurgy must go through this sintering process. Sintering is a procedure where the entire densification will take place and involves the development of new ceramic structure. To ensure that the diffusion mechanism of compressed loose particles occurs, this process must be carried out at temperatures close to the melting point of the ceramic[3].

The diffusion transport of materials at the interface of stacked or closed particles is a frequent mechanism for sintering. The diffusion process causes an interaction between pores and grain boundaries, which results in grain growth movement and the formation of a new dense grain structure. The particles are coalesced by solid state diffusion at this stage, with significant pore growth and grain growth development, causing by the presence of a high sintering temperature (figure(1.1))[3].

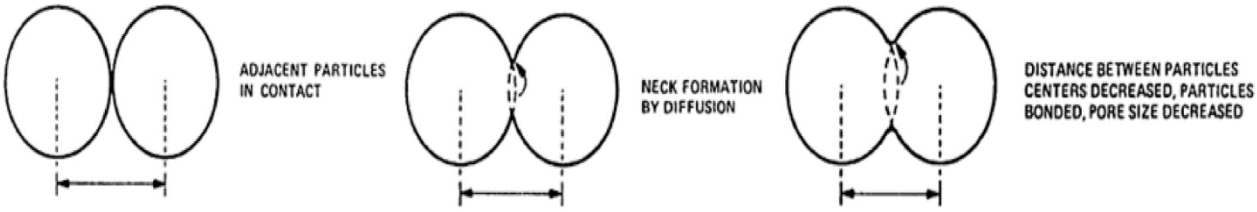

Figure (1.1): Schematic of Solid State Material Transport by Diffusion[3].

Ceramics with undesirable properties including low strength and cracking is result from uncontrolled grain growth. As a result, one of the most important processes in the construction of a good ceramic structure is controlling grain growth during the sintering stage. Because the final grain size and grain structure formation are directly regulated by grain growth, the required properties can be accomplished by increasing the diffusion distance for matter transport and therefore limiting the rate of grain growth. Normal and abnormal grain growth

are two types of grain growth in ceramic materials. As a result, suppressing abnormal grain growth is critical for generating a more homogeneous and denser product. In general, reducing grain growth rate and increasing densification rate, or a combination of the two, is required for the fabrication of ceramics with high density and controlled grain size. The employment of additive (dopant) in order to obtain the desired result is one of the adaptations of fabrication approaches that satisfy one or both of these conditions[3].

The choice of additives and dopants used in sintering, which affects the distribution of grain size and the phases generated in the grain boundary, influences the mechanical characteristics of alumina. Dopants are known to inhibit grain boundary movement and aid in the process of sintering. Magnesia (MgO), for instance, has been investigated because it speeds up densification, enabling the creation of a microstructure with uniform grain size, slows down grain growth, and increases the final density of alumina during sintering behavior that is beneficial for enhancing alumina's properties[2].

Engineering material failure is one of the most essential scientific subjects of all time due to the high cost of unfavorable damages and accidents. Engineers are frequently needed to comprehend the causes of failures and attempt to reduce the likelihood of failure in designed components. Cracks can be found all around us, and they can be caused by industrial defects or a range of environmental circumstances during loading. The most essential characteristics in fracture mechanics are crack opening displacement and crack propagation[4].

Fracture mechanics is the discipline that describes how a fracture or fault forms and propagates in a structure under applied loads. Because cracks can appear anywhere, fracture mechanics has a wide range of applications. Fracture mechanics is widely studied in many sciences and engineering disciplines[5].

It's difficult to measure crack opening displacement, and when values are smaller, special equipment is required. For a ceramic, SEM and AFM have been used. To establish correct displacement values, these procedures require precise sample preparation and special care[6,7]. To circumvent these challenges, a non-contact optical approach called Digital Image Correlation (DIC) can be utilized to quantify the displacement and strain of a sample in order to detect fracture propagation and assess crack opening displacement[8].

1.2 Aims of the Thesis

The need for ceramics with high performance in multiple applications, as well as somewhat low cost, has prompted this work, which has the following goals:

1- Investigation the effect of MgO with (2, 4, 6, 8, 10 wt.%) on the physical properties (density, porosity), mechanical properties (young's modules, passion ratio, hardness, fracture toughness), and microstructure of alumina.

2- Using digital image correlation to observe initiation of crack in Alumina-Magnesia samples, and observing the development of crack in the samples and the crack is visualized by their strain map.

3- Building an optimization model to get the optimum conditions of production process to get a desired properties.

1.3 Thesis Outline

This thesis consists of from six chapters. Chapter one gives an introduction to the thesis and describes briefly the materials used and its application and the goal of the thesis, chapter two includes the theoretical aspect of material and its structure and applications. The theoretical part also includes a brief history of fracture mechanics and the technique used to study the crack opening and propagation; this chapter also shows the literature review related with our work.

Chapter three explain a brief of an optimization technique. Chapter four deals with the experimental work through preparation of material and production and preparation of sample for test and explain how digital image correlation method used to study crack opening and propagation of sample. Chapter five shows the result of experimental work. Finally, Chapter five consists of the conclusions and suggestions for the future works.

Chapter Two

Theoretical Part and Literature Review

2.1 Introduction

This chapter covers the definition of Alumina, their properties and applications; the effect of Magnesia addition; an overview of toughening mechanisms; the approach used in fracture mechanics to determine the toughness; a summary in Digital Image Correlation analysis; and a literature review on the thesis's topic.

2.2 Alumina (Al_2O_3)

α-Al_2O_3 has the highest hardness and density among aluminum oxides that is formed by heating of other polymorphs of alumina or alumina hydrate at a high temperature. Additionally, α-alumina can be produced by melting process of alumina hydrate at up to more than 2000°C and subsequently its cooling and crushing. Another reason alumina is significant compared to other engineering oxide ceramics is due to a lower sintering temperature which makes it economical[9].

2.2.1 Structures of Alumina

Tables (2.1) provides information on the structures of alumina. Corundum is the sole stable form of Al_2O_3 at all temperatures. In figure (2.1), the corundum structure is displayed. It comprises of oxygen ions packed closely together in a space group R3c hexagonal (rhombohedral) lattice. In the oxygen lattice, the aluminum ions occupy two-thirds of the octahedral positions. The corundum

lattice characteristics in Table (2.1) correspond to a hexagonal unit cell with 12 Al_2O_3 molecules. The parameters of the rhombohedral lattice are a = 5.128 A° and α= 55.28°[10].

Table (2.1) Structures of stable alumina (corundum) and unstable alumina[10].

Designation	Structure	Lattice Parameters, angle (A°)		
		a	***b***	***c***
Corundum	Hexagonal (rhombohedral)	4.758		12.991
Eta	Cubic (spinal)	7.90		
Gamma	Tetragonal	7.95		7.79
Delta	Tetragonal	7.97		23.47
Theta	Monoclinic	5.63	2.95	11.86 103° 42’
Kappa	Orthorhombic	8.49	12.73	13.39

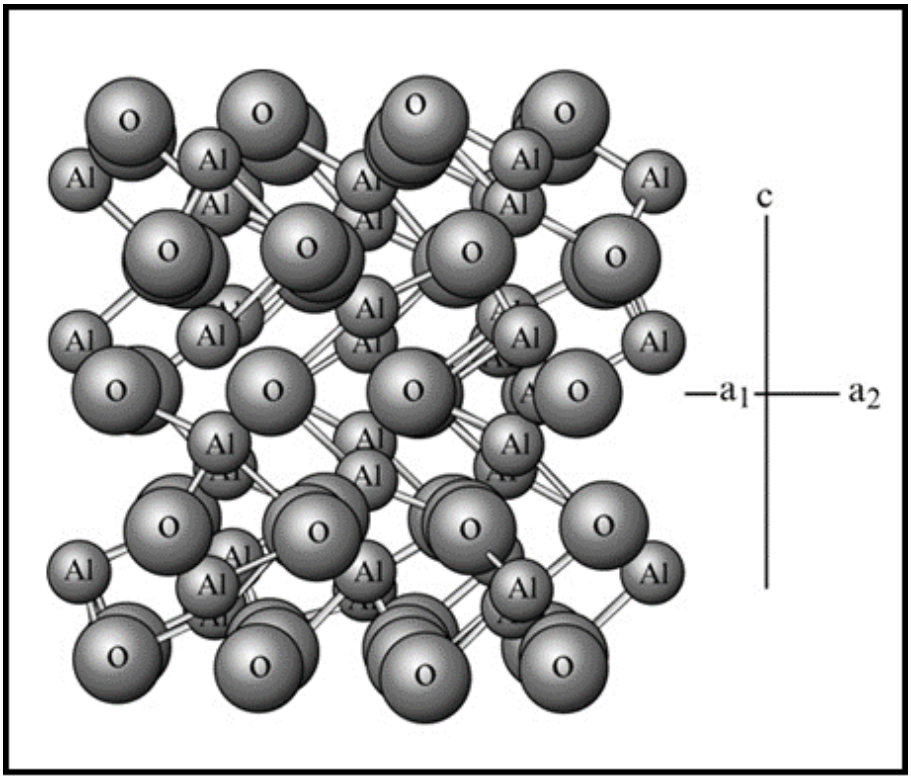

Figure (2.1) The structure of corundum (alpha-alumina) from atoms occupy two-thirds of the octahedral interstices in a hexagonal close-packed array of oxygen atoms, which is distorted because the octahedral share faces in pairs[10].

In comparison to corundum, all of the different metastable alumina forms are less dense. Other allotropic structures have been proposed, although they lack the same level of confirmation as those in Table (2.1). This metastable alumina all have almost close-packed cubic oxygen packings. Eta or gamma alumina often occur at low temperatures and change with increasing temperature in the order gamma → delta → theta → alpha alumina. There are also more variations that are conceivable, such as gamma that is produced at greater temperatures and converts immediately to alpha. Particle size, heating rate, contaminants, and environment are a few examples of variables that might affect the kinetics of transformation and the order of phases. Only alpha phase (corundum) is often found over 1,200°C[10].

2.2.2 Physical Properties of Alumina

The microstructural characteristics of alumina, which may occur in several metastable phases and permanently convert into alpha-alumina when heated over 1200◦ C, make it a biomaterial. Alpha alumina is a thermodynamically stable phase made up of a closely packed hexagonal arrangement of oxygen ions. The material used for biomedical applications is alpha-alumina (also known as corundum or emery if impurities are present)[11].

The high melting point, hardness, and resistance to attack by powerful inorganic acids of alumina are due to strong ionic and covalent chemical interactions between Al^{3+} and O^{2-} ions in the alumina molecule. In other words, alpha-alumina is aluminum metal in its most oxidative form, with exceptional chemical and physical stability: it is particularly resistant to strong inorganic acids such as orthophosphoric or hydrofluoric acid. The energy of the ionic-covalent bonds in the solid is also responsible for the solid's low electric and thermal conductivity and high melting point[11].

2.2.3 Mechanical Properties of Alumina

Alumina, like other ceramics, has a brittle fracture characteristic and moderate tensile and bending resistance. There is no yielding at the tip of fractures in alumina, unlike metals, to relieve tension. Surface imperfections, notches, and internal faults are unavoidable and enhance stress concentration locally. Tensile forces, in particular, promote the expansion of flaws to the point where they become genuine cracks and ceramic fractures. The fundamental constraint in developing alumina components is its brittle fracture characteristic (poor toughness)[11].

This behavior can be influenced by choosing a high-purity raw material, or by reducing grain size (which means smaller grains), and increasing density (meaning less porosity, less flaws)[11]. Table (2.2) shows the mechanical properties of Alumina (>99.5% purity)[12].

Table (2.2) Mechanical properties of Alumina (Al_2O_3) ceramic[12]

Parameters	Unit of measures	Values
Density	gm/cm3	3.85
Flexural strength	MPa	379
Elastic modulus	GPa	375
Shear modulus	GPa	152
Bulk modulus	GPa	228
Compressive strength	MPa	2600
Tensile strength	MPa	275
Hardness	Kg/mm2	1440
Thermal conductivity	W/moK	35
Fracture toughness	MPa$\sqrt{m}$	4.0
Coefficient of thermal expansion	$\times 10^{-6}/^{o}C$	8.4

2.2.4 Applications of Alumina

Alumina is helpful due to a number of its characteristics. It may be used as high-temperature components, catalyst substrates, and biomedical implants because of its high melting temperature of 2,054°C and chemical stability and unreactivity. Alumina is suitable for abrasive materials, bearings, and cutting tools because it has among the greatest levels of hardness, strength, and abrasion resistance among oxides. Due to alumina's strong electrical resistance, it is employed both in pure form and as an ingredient in electrical insulators and other components. Alumina has exceptional optical transparency, making it crucial as a gem stone (sapphires and rubies) and a laser host when combined with additions like chromium and titanium (ruby). Given that it has a high melting point, is chemically inert, and is transparent to light, it is highly useful for containing arcs in street lamps. See Table (2.3) for more on uses of alumina[10].

Table (2.3) Uses of Alumina[10].

Solid alumina	*Alumina powders*	*Alumina coatings*	*Alumina fibers*	*Alumina as a component*
Furnace components	Abrasives	Oxidation protection of aluminum and aluminum alloys	Thermal insulators	Ceramics and glasses
Catalyst substrates	Catalyst pellets	Capacitors	Fire retardation	Mullite components
Electronics substrates		Transisitors		Electrical insulators
Electrical insulators		Bioceramics		Porcelains
Cutting tools				Durable glasses
Bearings				
Spark Plugs				
Arc lamp tubes				
Laser hosts				
Gem stones				

2.3 Magnesia

With a high melting temperature (2,800°C), alkaline-earth elements can form oxides with the general formula MgO. The most frequent minerals that include these elements are calcite ($CaCO_3$) for calcium, magnesite ($MgCO_3$) and its hydrated forms for magnesium, and dolomite $(CaMg)CO_3$, which contains both cations. This is due to their reactivity with water and susceptibility to carbonation. (1.3 $kg.m^{-3}$, in the form of chlorides and sulphates), and hydrated magnesia $Mg(OH)_2$ may be recovered by treating seawater, which also contains a sizeable amount of magnesium. The iron and steel industry, which requires the material's essential oxide characteristics, uses the majority of the magnesia produced for refractories. Magnesium withstands the 1,700°C temperatures of converters, where it can dissolve iron oxide up to several times its weight without melting and successfully fends off slag assault and sealing[13].

2.4 Effect of Magnesia Addition

Uncontrolled grain development is a serious issue that causes ceramics to have undesired qualities such as poor strength and cracking. As a result, one of the most important processes in the construction of a good ceramic structure is controlling grain growth during the sintering stage. Because the ultimate grain size and grain structure formation are directly regulated by grain growth, the required qualities can be accomplished by increasing the diffusion distance for matter transport and therefore limiting the rate of grain growth. Normal and abnormal grain growth may be distinguished in ceramic materials[14-16]. Controlling abnormal grain growth is therefore critical for producing a uniform and greater density. Basically, lowering grain growth rate and increasing densification rate, or a combination of the two, is required for the fabrication of high density and regulated grain size ceramics. The employment of additive (dopant) in order to get the desired is one of the variations of manufacturing procedures that meet one or both of these conditions[17-19]. In fact, using

additives to fabricate a pressureless sintering ceramic with a high density and grain size structure is a very successful method[20]. To achieve the desired result, a little quantity of additive was doped into Al_2O_3 compacted pellets as a sintering aid. In general, additives like MgO, TiO_2, ZrO_2, Y_2O_3, and Li_2O_3 are often employed in ceramic systems to impact the densification process by lowering the sintering temperature and duration, inhibiting and stimulating grain development, and improving physical and mechanical characteristics[18-22]. A minor amount of MgO is well recognized for inhibiting discontinuous grain formation and promoting Al_2O_3 sintering, resulting in a totally dense and strongly finer homogenous structure[21]. The binary phase diagram for $MgO-Al_2O_3$ is simple. There is only one stable intermediate compound that of the spinel phase (Mg_2AlO_4). Spinel melts at 2,105°C, but there is a eutectic at 1,995°C and a limited solid solution between stoichiometric spinel and MgO (periclase), up to 6 wt% MgO, can be dissolved into the spinel structure without exsolution. This limited solid solution is an important property that is utilized in manufacture of spinels for use in reducing conditions[10]. Figure (2.2) shows the Alumina-Magnesia phase-diagram[23].

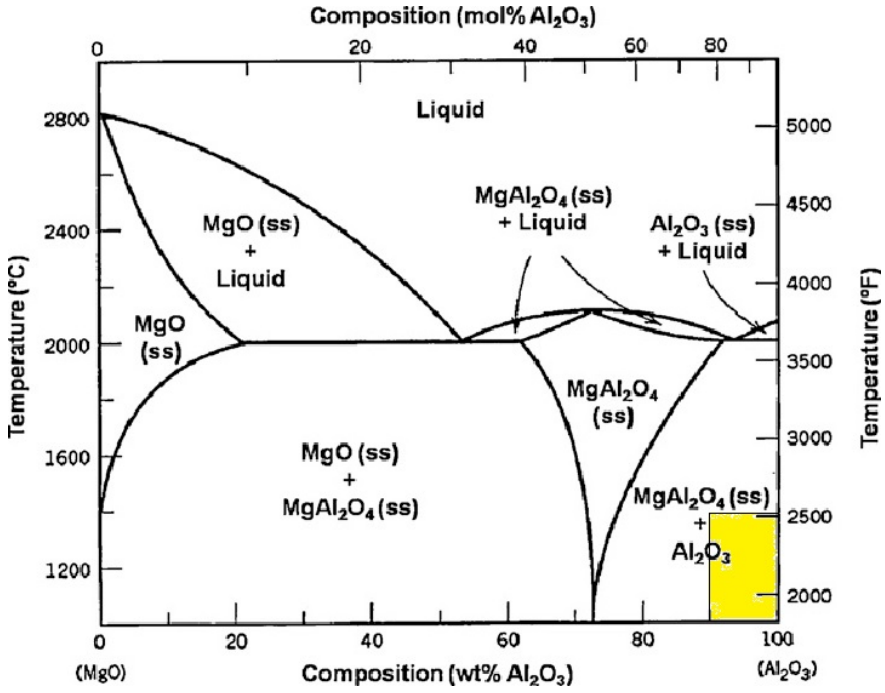

Figure (2.2): Alumina-Magnesia phase-diagram[23]

2.5 Toughening Mechanisms

Before going over various ceramic's toughening mechanisms, it's vital to go over the topic of brittleness in ceramics. Ceramics' brittleness has long been recognized as the result of a variety of circumstances[24].

When dislocations cannot glide on all available slip planes as ions displacements in ceramics with mainly ionic binding, the local electrical charge neutrality criterion might be violated. As a result, dislocations must only be able to glide on certain planes aligned at a 45° angle in order to reestablish electroneutrality, figure (2.3a)[25].

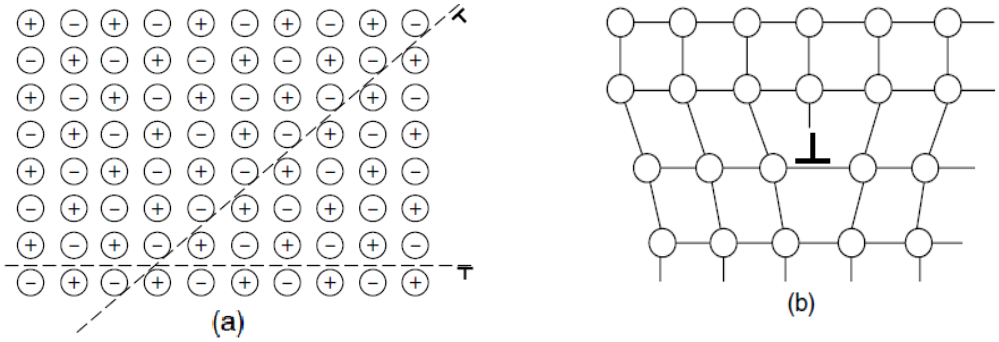

Figure (2.3): Schematic illustration showing (a) the possibility of dislocation glide at specific planes in an ionic ceramic and (b) the difficulty in dislocation glide due to rigid bond network in a covalent ceramic[25].

Dislocation movement in ceramics with primarily covalent bonds is problematic due to directional features and the naturally stiff bond network, as movement necessitates bond breaking and remaking, as well as distorted bond angles (Figure 2.3b)[25].

Ceramics have a shorter dislocation core width than metals, which necessitates a high Pierls–Nabarro stress for dislocation glide[26].

All of the aforementioned variables make it difficult for a ceramic grain in a limited microstructure to accept shape change; otherwise, strain

incompatibilities at the grain boundary led to cracking. It is quite easy for cracks to form in ceramics once cracking begins. In metals, yielding or localized plasticity as a result of dislocation movement in the fracture tip stress field occurs. This absorbs a portion of the available energy at the fracture tip, lowering the total driving power needed to propagate the crack farther in metals. Because ceramics lack dislocation glide, such a phenomenon is ruled out; as a result, if fractures reach a critical size, they frequently expand in an unstable way, leading to fracture or failure of the ceramic component. Due of the absence of room-temperature ductility, the ceramics community has been working hard to develop innovative microstructural designs to improve crack development resistance. From a basic standpoint, any interaction between a developing fracture and the microstructure that can absorb a percentage of the energy available at the crack tip stress field reduces the driving force for crack propagation. In other words, the crack opening displacement will be minimized, and the crack tip will be blunted as a consequence. Toughening processes, or methods that increase fracture development resistance, can be generically categorized into two kinds (Figure 2.4)[25].

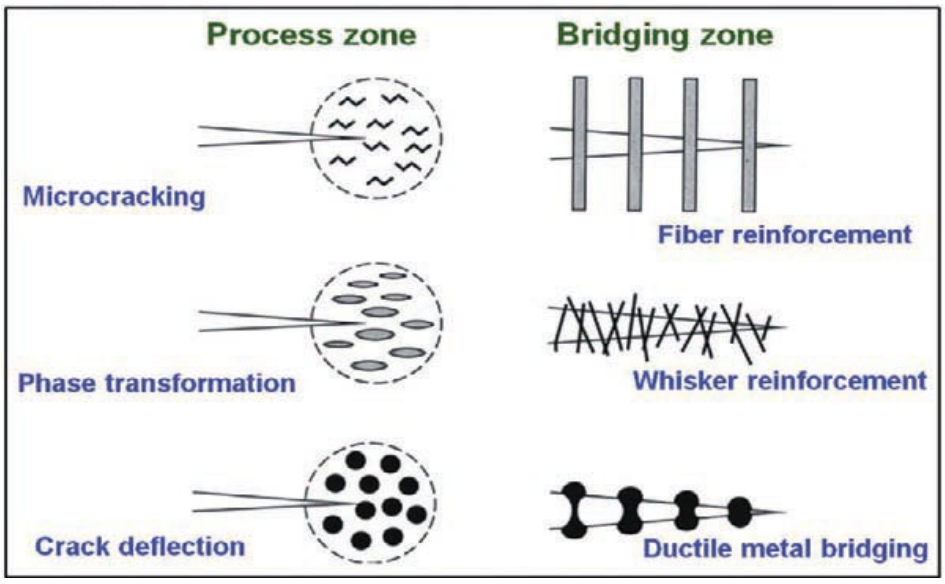

Figure (2.4): Summary of various toughening mechanisms in ceramic-based materials[24].

Phase-transformation-induced volume expansion, microcracking, or crack deflection in the process zone near the fracture tip result in enhanced crack growth resistance. When phase transition results in toughening (popularly known as transformation toughening), For instance, the crack tip stress field volume expands when zirconia changes from tetragonal to monoclinic. This will provide compressive stress on the fracture faces in a restricted microstructure, which will cause the crack tip to close. In composites with particles, whiskers, or fibers as the second phase, crack deflection is most frequently seen[25].

Numerous studies have demonstrated how the microstructure of alumina-based ceramics affects their behavior, with the majority of these studies concentrating on the effect of grain size. It is well known that alumina's resistance typically improves with smaller grain size and a narrow range of particle size distribution. Several publications that concentrate on the modes of wear, such as erosive, abrasive, cut, and milling, reveal similar connections between the rates of wear and grain size. In order to understand how alumina's grain size affects wear, it is clear that a number of factors, including the manufacturing process, the timing and technique of sintering, and the introduction of a second crystallin phase, affect this property. and dopant’s concentration[2].

2.6 Fracture Toughness Measurement

It's important to remember that the toughness of brittle materials is determined by the testing methodology, which is divided into long crack and short crack ways. The single edge notched beam (SENB) and single edge V-notched beam (SEVNB) approaches are two long crack methods. The fracture

lengths (radial–median) surrounding hardness indentations are measured using short crack procedures, and the toughness data is estimated using several described models. While the research on indentation-induced damage behavior is relevant to wear resistance, the indentation technique is frequently used to assess the toughness or fracture development resistance qualities of ceramics. It should be emphasized that indentation techniques cannot be used to determine the absolute toughness of brittle materials; instead, long crack fracture toughness measurement techniques such as SENB, SEVNB, and chevron notch beam must be used (CNB). The indentation technique, on the other hand, is frequently used to compare the toughness qualities of freshly designed composites. Furthermore, it is now commonly understood that careful application may produce repeatable indentation toughness data. It's worth noting that the indentation method is now commonly used to calculate the fracture toughness of tiny and moderately brittle materials that are difficult to manufacture into typical test samples (e.g., SENB, SEVNB)[27-31].

In general, there are two methods for determining the fracture toughness of brittle materials. One approach is to use long cracks to measure toughness, while the other is to use short crack ways to evaluate toughness[25].

a- Long Crack Methods.

b- Fracture Toughness Evaluation Using Indentation Cracking.

2.6.1 Long Crack Methods

The most challenging aspect of doing long crack fracture toughness testing on ceramics is preparing a sharp crack in front of the notch[25]. Precracking the ceramic material is often done in one of two ways[26]:

(a) SENB Method. Cyclic compressive stresses are given to a SENB specimen with a cut notch in this sample. When the sample is loaded in flexure

mode, this causes damage buildup and fracture propagation in the zone ahead of the notch[25]

SENB uses the following formula to calculate the mode I critical stress intensity factor (KIC)[25]:

$$\mathbf{KIC} = \boldsymbol{Y}\left(\frac{\boldsymbol{3Pc}}{\boldsymbol{h^2 d}}\right)\boldsymbol{c^2} \qquad \text{..... (2.1)}$$

Where Y = 1.99 – 2.47(c/h) + 12.97(c/h)^2 – 23.17(c/h)^3 + 24.8(c/h)^4.

P, c, **d**, **h**, are fracture load, precrack length, specimen width, and specimen thickness as showing in figure (2.5).

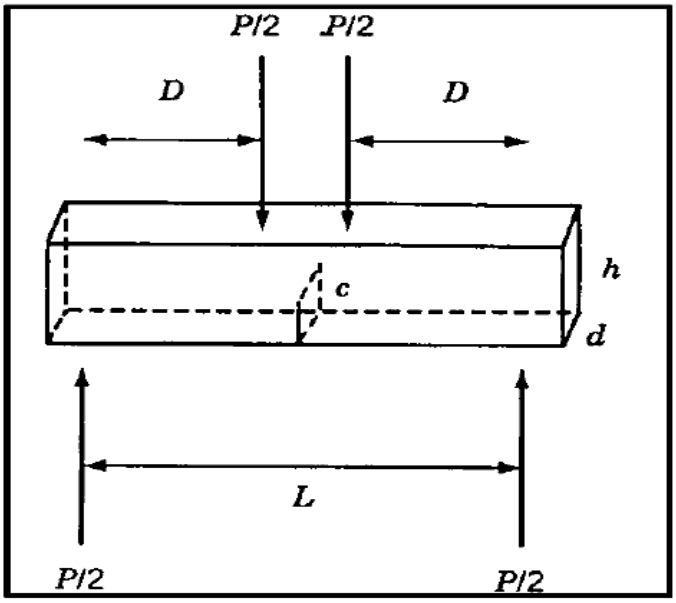

Figure (2.5): Typical geometry and loading configuration involved in SENB testing to evaluate fracture toughness [24].

(b) SEVNB Method. This is an improved variation of the SENB technique, in which the notch root is polished using a razor blade filled with diamond paste to form a crisp "V" notch. Rectangular samples obtained using the previously stated procedure are utilized in the SEVNB method to measure the fracture toughness of the materials (figure (2.6)). On a commercial V-notch preparation equipment, a V-shaped notch was inserted along the height of the

specimen using a diamond saw and razor blade with diamond abrasive. The radius of the notch might be smaller than 10μm. After that, the samples are cracked on a UTM utilizing a four-point bending arrangement[26]. The fracture load is measured, and fracture toughness is estimated using the equations below[32,33]:

$$\mathbf{KIC} = \frac{\mathbf{Pf}(L_0 - L_i)}{BW^{3/2}} \frac{3\alpha^{1/2}}{2(1-\alpha)^{3/2}} \mathbf{f}(\alpha) \qquad \text{..... (2.2)}$$

where $\mathbf{P_f}$, $\mathbf{L_0}$, $\mathbf{L_i}$, **B**, and **W** are fracture load, outer span, inner span, specimen width, and specimen thickness, respectively, $\boldsymbol{\alpha} = \mathbf{a/W}$ with **a** the precrack size, and $\mathbf{f(\alpha)}$ is:

$$\mathbf{f}(\alpha) = 1.9887 - 1.326\alpha - \frac{\alpha(1-\alpha)(3.49-0.68\alpha+1.35\alpha^2)}{(1+\alpha)^2}$$

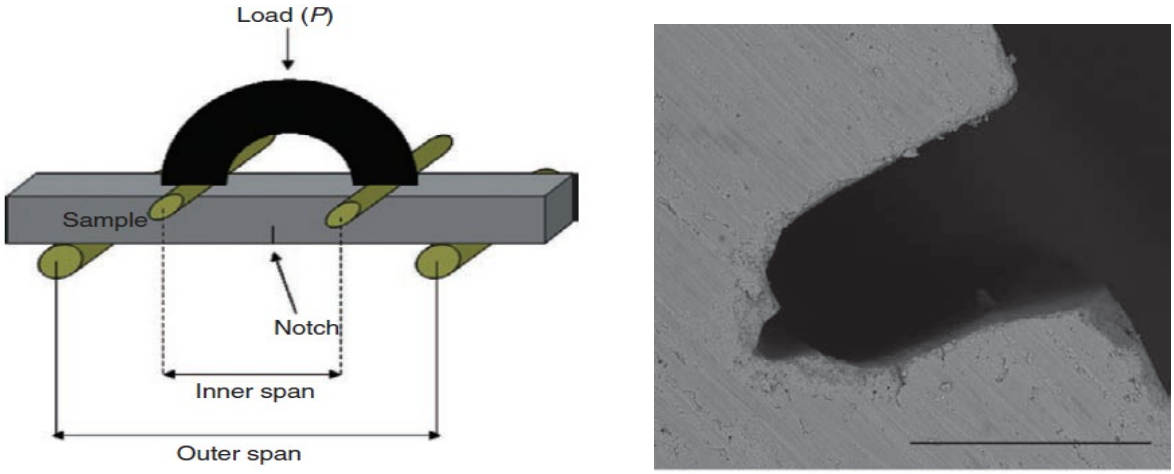

(a) **(b)**

Figure (2.6): a) Four-point flexural configuration for SEVNB testing of fracture toughness measurement, b)V-notch image[25].

2.6.2 Fracture Toughness Evaluation Using Indentation Cracking

Hardness indenters can create small surface fractures with regulated size and sharpness in fragile materials like ceramics. This is especially true in ceramic tribological applications, where the short crack fracture toughness has a

greater impact on wear behavior. This is especially relevant because many ceramics exhibit microcracks and subsequent spalling on worn surfaces[34]. It's also a good idea to test the toughness of ceramics with novel compositions at different weights to see if toughness rises with fracture length, resulting in "R"-curve behavior[25].

(a) Indentation Microfracture (IM) Method. When the residual stress driving force (K_{res}) at the crack tip is in equilibrium with the fracture toughness, the median cracks that emerge from the corners of a Vickers indentation are stopped[25]:

$$\boldsymbol{KIC = \chi\left(\frac{P}{c^{\frac{3}{2}}}\right) = K_{res}} \qquad \text{..... (2.3)}$$

where KIC is the indentation fracture toughness (Pa $m^{1/2}$), E is the elastic modulus (GPa), H is the Vickers hardness (GPa), P is the indentation load (N), χ is the residual stress factor, and c is the crack length (m) measured from the center of the indent impression[25].

(b) Indentation Strength Bending (ISB) Method. In this approach, a Vickers indenter is put in the middle of a beam specimen's tensile surface, and the specimen is then bent to failure. The diameters of the radial cracks are measured visually. To prevent environmentally assisted subcritical development, a drop of silicon oil was applied to the indent. On the tensile surface, the specimen surfaces with microcracks are loaded[25].

Using Chantikul et al.'s the fracture toughness is calculated from the strength and indent load[35]:

$$\boldsymbol{KIC = 0.59\left(\frac{E}{H}\right)^{1/8}(\sigma P^{1/3})^{3/4}} \qquad \text{..... (2.4)}$$

where σ is the failure strength, E is the elastic modulus, P is the indentation's load.

2.6.3 Crack Opening Displacement (COD)

COD, originally known as "crack opening displacement," is related to LEFM by the recognition that there is a "plastic zone" around the crack tip in any real material, necessitating modification of the purely linear model[36,37].

Crack opening displacement (COD) is a parameter used to describe and predict the near-tip crack profile. It is defined as a movement of the upper and lower crack flanks relative to one another[38].

When the displacement is measured near the crack mouth, it is referred to as "Crack Mouth Opening Displacement (CMOD)," and when it is measured at the intersection of a 90° vertex with the crack edges, it is referred to as "Crack Tip Opening Displacement (CTOD)"[39]. see Illustration (2.7)

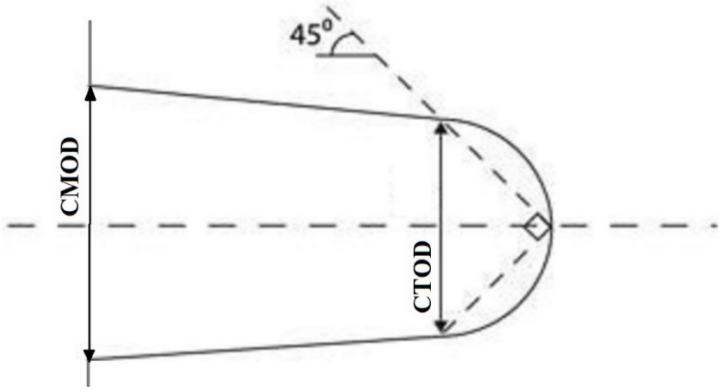

Figure (2.7): COD [40].

2.7 Digital Image Correlation

DIC is a non-contacting optical and numerical technique that can precisely measure two-dimensional (2-D) and three-dimensional (3-D) displacements and stresses throughout the whole field of view. By analytically comparing comparable local characteristics in images of an item's surface taken before and after deformation, it is possible to determine how much an object has changed.

The approach is appropriate for both laboratory and field applications since images are frequently taken in settings with natural or white light. The approach may be used to a wide range of length scales, from the macro to the nanoscale[41,42].

To achieve the utmost accuracy in the tracking algorithms, a high contrast random pattern is often put to the surface of a specimen. Spraying black and white paint specks on the specimen surface can quickly produce this pattern. Images are frequently captured using black and white cameras or changed to greyscale[43]. This makes sure that each pixel of the applied surface pattern is numerically represented in the digital space as illustrated in figure (2.8). Numerous mathematical methods have been devised to precisely trace the deformations in these digital pictures, for both 2-D and 3-D deformations, down to the sub-pixel level[44].

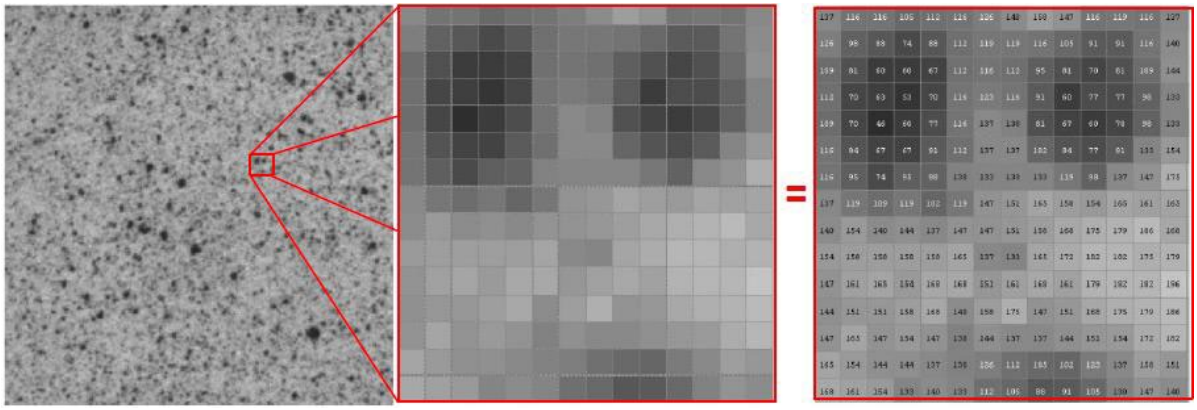

Figure (2.8): Digital representation of surface speckle[44].

Three stages are often involved in DIC: setting up the experiment and preparing the samples, acquiring the images, and analyzing the results. The processing of specimens is not too difficult. The specimen's surface must have a random pattern for DIC to work. A thin coat of black and white paint is often used to apply this pattern, which can also appear naturally on the surface of the specimen. For the analysis to generate the most precise results, this pattern must

have a number of features. As the bearer of the displacement information, the specimen surface must first deform when this random pattern is applied. Because the recorded changes in light intensities reflecting from this pattern serve as the foundation for DIC analysis, this random pattern should likewise be highly contrasted. To properly resolve this pattern, the speckles or dots inside it must also be of an acceptable size in relation to the camera's pixel resolution. To get the most precise results, the camera(s) must be correctly set up once the specimen is properly prepared[45].

2.7.1 DIC Analysis Principles

Computer algorithms are utilized to compare sequential digital images once the specimen deformation photos have been obtained. Figure (2.9) depicts the main goal of DIC analysis. The comparable position P' (x_o', y_o') in a distorted picture is found by choosing a subset of M pixels that is centered at the point P (x_o, y_o) in the reference image. As can be seen, this offers sufficient details to compute the displacement vector of the point (P)[46].

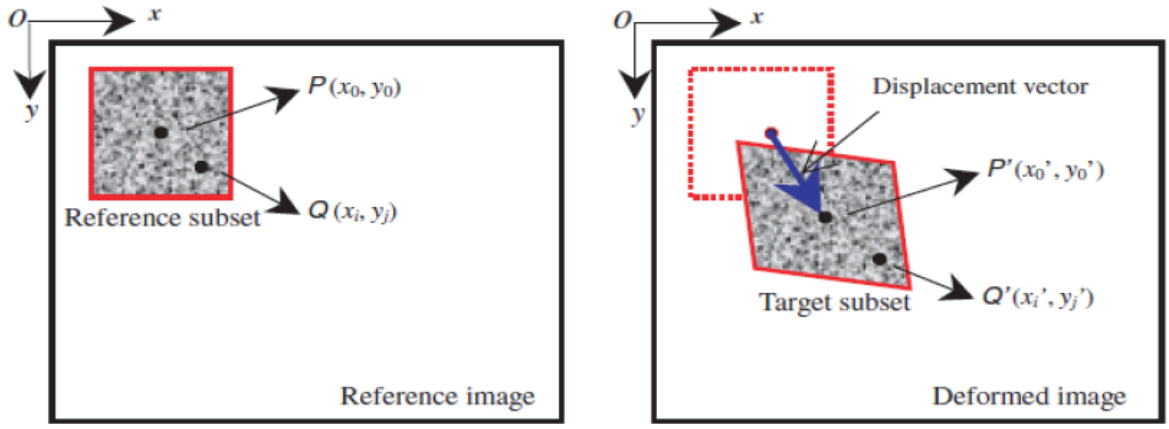

Figure (2.9): DIC subset matching[46]

The reference picture is often broken into several subsets, and the distances between these subsets are chosen based on the results' needed spatial resolution. A full-field displacement map is created once all of the subsets in a region of interest have been located at their appropriate locations. A predetermined

correlation criteria and sub-pixel technique must be used to accurately compute these displacements. The cross-correlation, as given in the equation below, is the most widely used criterion[47]:

$$C_{cc} = \sum_{i=-M}^{M} \sum_{j=-M}^{M} [f(x_i, y_j) * g(x'_I, y'_j)]$$

where f and g are the reference and deformed image functions, respectively.

The multiple subsets of pixels used by DIC algorithms rather than a individual pixels are used to calculate displacement. The reason for this is because there are only a limited number of methods to represent pictures in digital form[42].

2.8 Literature Review

2.8.1 Toughening of Alumina.

Zawati Harun et al. (2012) investigated the influence of MgO additive on Al_2O_3 microstructure and physical qualities. They created compacted alumina pellets by sintering various alumina particles (25µm and 90µm) together. To densify the final ceramic structure, the consolidation was additionally aided by the sintering aid (0.25wt percent MgO). The impact of additive on the different particle sizes of compacted alumina was then compared by evaluating the microstructure and physical characteristics. When the bulk density and apparent porosity are measured, the findings reveal that the pellet sintered for 2 hours with particle size 25µm has a greater bulk density value than the pellet with particle size 90µm, and the usage of the 25µm particle results in a lower apparent

porosity value. These findings suggest that MgO might speed and increase densification during the sintering stage, resulting in a lower porosity value of the consolidated structure[3].

Mehran Dadkhah, et al. (2014) investigated the physical properties of sintered Alumina in the presence of MgO nanopowder. 0.1, 0.3, and 0.5 wt% of MgO are added to alumina in order to examine the impact of magnesia nanopowders on the physical characteristics of sintered alumina. The produced samples were sintered for four hours at 1570°C in an inert environment. The transmission electron microscope (TEM) and scanning electron microscope were used to determine the shape and size of nanopowders (SEM). X-ray diffraction and Fourier transform infrared spectroscopy (FT-IR) were used to study structural analysis (XRD). Results demonstrate that spinel phase ($MgAl_2O_4$) has been produced in the structure of alumina by increasing the fraction of MgO. Spinel phase diffused across the grain boundaries during the sintering process, pinning the grain borders, which resulted in a reduction in grain size. Therefore, by reducing the grain size, sintered alumina's physical characteristics have been enhanced[9].

Pâmela Milak, et al. (2015) Published a review study on alumina wear. Where I showed the factors affecting abrasive and erosive wear (material composition, characteristics of the used oxides, and the manufacturing process that defines the final microstructure) and the effect of particle size on the wear rate of alumina and how to control particle growth during the sintering process using doping and thus affecting the mechanical properties and physical of the product. It is known that the small grain size and a narrow strip of particle size

distribution generally promote an improvement in the resistance of alumina wear. Aiming to approach the influence of grain size about the wear of alumina, it can be seen that various factors interfere on this characteristic like the route of fabrication, method and time of sintering, introducing a second crystalline phase in the material, and concentration of dopants[2].

Pittari, J., et al. (2015). The quasi-static fracture toughness (KIC) of pressureless sintered and reaction-bonded silicon carbide (SiC) ceramics was investigated using a four-point bend, a chevron-notch testing method. ASTM C1421 Testing Standard Configuration A is met by the sample geometry. The tests were carried out using an electro-mechanical universal testing machine. To validate steady crack nucleation and growth, the crack mouth opening displacement was measured using (DIC). Because of the presence of silicon phase, which has a quasi-ductile fracture behavior, the reaction-bonded composite had a higher KIC value than the pressureless sintered ceramic, which could be advantageous for applications requiring ceramics that are less brittle[48].

Ali Arab et al. (2019) explore the influence of MgO addition on the mechanical and dynamic characteristics of conventionally sintering Zirconia Toughened Alumina (ZTA) Ceramics. ZTA composites' microstructure and mechanical characteristics were studied. Because of the pinning effect of MgO and the decrease in porosity in the microstructure, the hardness of ZTA composites enhanced for less than 0.7 wt.% percent MgO. The fracture toughness of ZTA composites, on the other hand, has been steadily decreasing

due to the size reduction of Al_2O_3 grains. This is the primary cause of a decrease in dynamic compressive strength greater than 0.2 wt.% percent MgO addition. As a result, the SHPB test demonstrates that adding 0.2 wt.% percent MgO to ZTA ceramics improves dynamic compressive strength just somewhat. FESEM images of ZTA-MgO samples (Figure (2.10)) validated the phase compositions, demonstrating that the Al_2O_3 particle size decreases with increasing MgO addition. The pinning action of MgO caused the reduction in Al_2O_3 particle size. MgO was found in the grain development of Al_2O_3. This mechanism can be explained by (I) decreasing grain boundary anisotropy and surface energy of grains; (II) increasing pore mobility due to an increase in surface diffusivity; (III) increasing densification rate by promoting lattice and boundary diffusions[1].

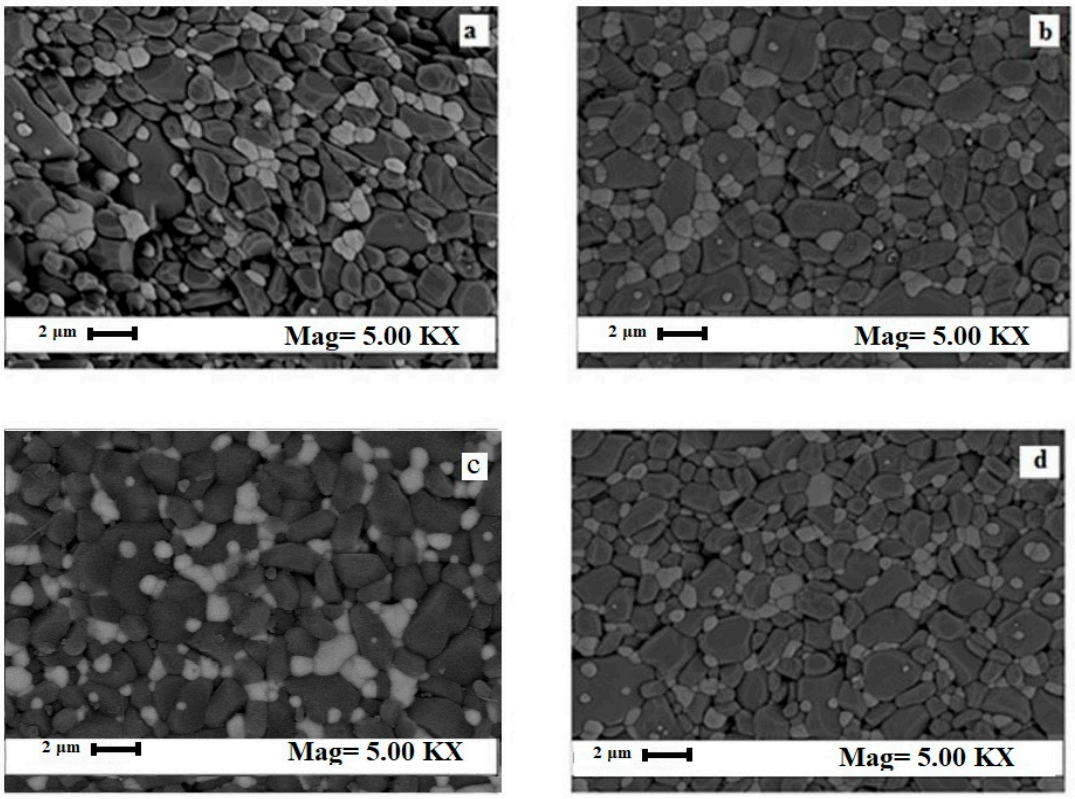

Figure (2.10). Microstructure of ZTA-MgO samples. (a) 0.2 wt.% MgO, (b) 0.5 wt.% MgO,(c) 0.7 wt.% MgO, and (d) 0.9 wt.% MgO[1].

2.8.2 Investigation fracture behavior by DIC.

Tomasz Brynk et al. (2013) used digital image correlation to explore the stress intensity factor values of brittle materials. The material employed is WC with 40% Co, and two separate testing methodologies were applied. First, a technique for testing notch samples using three points (SENB). The method combined cyclic loading of samples with the DIC technique. The second test involved calculating stress intensity parameters directly from displacement field measurements at the notch tip. The results of the stress intensity factor using DIC displacement field measurements match well with the results of the SENB approach[8].

Qing Lin, et al. (2013) integrated the fracture characterization of sandstone using digital image correlation (DIC) technique. Digital image correlation tests were conducted to identify deformation with micronscale resolution. Displacement is obtained by comparing a pair of digital photographs and matching a tiny region from the image before to distortion to the image following deformation. The Berea sandstone was subjected to I fracture testing employing three-point bending. Twelve specimens of three different types were created: six with a 0.5mm radius center notch, three with smooth boundaries, and three with reduced sections (6 or 12mm radius notch). A comprehensive displacement measurement was used to obtain the tensile fracture properties, such as crack opening displacement and crack length. The critical opening displacement (COD) for the center notch specimens was 30 mm at the notch tip at the start of unstable propagation (peak load), and as the crack spread, the known location of the COD permitted the identification of the process zone throughout the post-peak response. The effective crack's tip and the length of the process zone, l_p=5-

7mm, or roughly 10 times the maximum grain size, were determined using incremental displacement contours. Additionally, it was noted that during all experiments, the process zone maintained a steady length and constant critical opening[47].

Mohammed M. Hussien, et al. (2017) integrated the fracture behavior of HA samples (crack observation, initiation, opening, and propagation). In this investigation, a single edge notched beam was subjected to a three-point bending test. The essential CMOD and CTOD were 40 and 17 μm, respectively, for a critical bending strain of about 10 N. Nucleation critical time was 210 seconds, and fracture toughness was 0.7 MPa.√m. The DIC method has been shown to be a reliable and accurate tool for assessing fracture parameters such as crack opening and crack length (figure(2.11))[49].

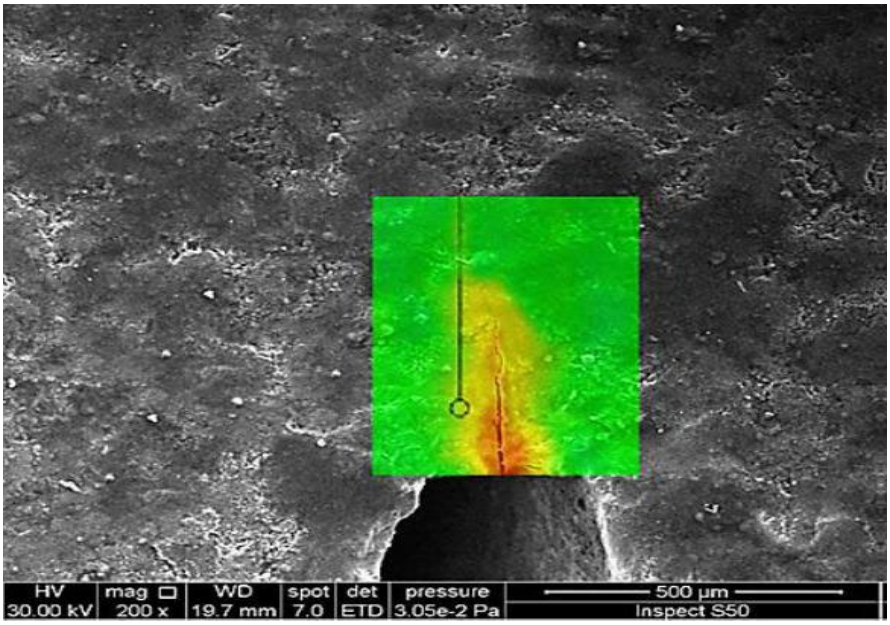

Figure (2.11). Correlation between SEM and DIC of HA specimen after bending test[49].

Hadeer S. Abd Ali, et al. (2021) integrated after adding (3, 5 wt. %) zirconia as reinforcement, the mechanical behavior (i.e. crack opening displacement and fracture toughness) of bioglass-ceramic. However, fracture

toughness was determined using a three-point bending approach. The DIC approach was utilized to observe fracture initiation, evaluate crack propagation of the bioactive glass-ceramic/zirconia composite, and calculate COD at the crack tip and mouth. The critical loads for pure bioactive glass, and glass/(3,5wt%) zirconia were determined (11, 15, 22 N). By inducing fracture branching and crack deflection (see figure) (2.13), zirconia particles boosted the toughness of composite bioceramics [50].

Mariam I. Oribi, et al. (2022) used the Hydroxyapatite as a bone replacement material due to its better biocompatibility. Because it closely resembles the bones and teeth, hydroxyapatite is commonly employed as a bioceramic material for human hard tissue implants. Because of its poor mechanical properties especially fracture toughness, synthetic hydroxyapatite is limited used in low-load bearing applications.

In this study, Hydroxyapatite was prepared from bovine femur bone due to economically and environmentally preferable. Hydroxyapatite with (5, 10, 15, 20 wt% partial stabilized zirconia) composite fabricated by powder technology method. The specimen was compacted under uniaxial pressing and sintered at 1250 C˚. The mechanical and physical properties of the composite samples were determined. The experimental results showed that (HA/5wt.% PSZ) has the highest value in the physical and mechanical properties than other ratios. where, relative density was 3 g/cm³, porosity (13%), Vickers hardness (3.8GPa), compression strength (98MPa), bending strength (43 MPa) and fracture toughness (1.1 MPa.√m).

Phase transformation of zirconia from tetragonal phase to monoclinic phase was responsible for the toughening mechanism of the composites as a result of existing the zirconia particles that worked as an obstacle in front of the crack tip[51].

Authors / Year	Ref .	Summery
Zawati Harun et al. (2012)	[3]	Investigated the influence of MgO additive on Al_2O_3 microstructure and physical qualities. By adding 0.25wt percent MgO to two particle sizes' Alumina, and investigate the influence of MgO additive on the properties of the products.
Mehran Dadkhah, et al. (2014)	[9]	Investigated the physical properties of sintered Alumina in the presence of MgO nanopowder. Results demonstrate that spinel phase (MgAl2O4) has been produced in the structure of alumina by increasing the fraction of MgO.
Pâmela Milak, et al. (2015)	[2]	Published a review study on alumina wear. Where I showed the factors affecting abrasive and erosive wear, and the effect of particle size on the wear rate of alumina and how to control particle growth during the sintering process using doping.
Pittari, J., et al . (2015)	[48]	The quasi-static fracture toughness (KIC) of pressureless sintered and reaction-bonded SiC ceramics was investigated to validate steady crack nucleation and growth, the crack mouth opening displacement was measured using (DIC).
Ali Arab et al. (2019)	[1]	Explore the influence of MgO addition on the mechanical and dynamic characteristics of conventionally sintering (ZTA) composite Ceramics.

Tomasz Brynk et al. (2013)	[8]	Used digital image correlation to explore the stress intensity factor values of brittle materials (WC with 40% Co). The results of the stress intensity factor using DIC displacement field measurements match well with the results of the SENB approach
Qing Lin, et al. (2013)	[47]	The Berea sandstone was subjected to I fracture testing employing three-point bending. A comprehensive displacement measurement was used to obtain the tensile fracture properties, such as crack opening displacement and crack length.
Mohammed M. Hussien and colleagues (2017)	[49]	Integrated the fracture behavior of HA samples. The DIC method has been shown to be a reliable and accurate tool for assessing fracture parameters such as crack opening and crack length
Hadeer S. Abd Ali and others (2021)	[50]	Integrated the effect of adding (3, 5 wt. %) zirconia as reinforcement, on the mechanical behavior of bioglass-ceramic. Zirconia particles boosted the toughness of composite bioceramics
Mariam I Oribi and others (2022)	[51]	Used the Hydroxyapatite as a bone replacement material due to its better biocompatibility, because it closely resembles the bones and teeth.

Chapter Three

Optimization Method

3.1 Experiments Design (DOE)

One of the most common methods for improving a process/product is experiment design. It is a statistical method that attempts to provide predictive knowledge of a complex process with many variables and few trials. The following are the primary DOE methods.

3 The Variance Analysis (ANOVA)

The variance Analysis (ANOVA) is a numerical method used to identify individual interactions for all control factors in the design test. ANOVA could be useful in determining the impact of input parameters and interpreting experiment data. By comparing the average square against the errors of experiment estimation at exact surety levels, ANOVA contributes to appropriately testing the significance of all major parameters and their interactions. Finally, a validation experiment should be performed to confirm the best parameters[52].

3.2 Design Expert

Design Expert is software that assists in the design and interpretation of multi-factor experiments. In the manufacturing process, we might use software to assist us in designing an experiment to see how a property like tensile strength varies with changes in processing conditions. The software includes a variety of designs, such as factorials, fractional factorials, and

composite designs. It is capable of handling both process variables. Design Expert provides computer-generated D-optimal designs in situations where standard designs are inapplicable or where we wish to augment an existing design, such as to fit a more flexible model[53].

State ease's Design Expert software is a statistical method. This was initially released in 1996 to aid in the execution of experimental designs such as determining the best formula for a preparation. In addition to optimization, software can interpret the factors in the experiment. This is divided into three research directions in software, depending on the experimental design to be carried out. There are options for screening, characterization, and optimization[54].

Screening takes the least amount of time to run but yields the least amount of information. The number of experiments that must be carried out in accordance with the chosen experimental design is referred to as the run. Screening is used when there are several possible factors (>6), but it is unknown which one has a real effect. Identifying several important factors with only two levels of each factor and estimating the main effect (no interaction). Follow-up with the second DOE is required to estimate interactions and additional requirements[54].

Characterization necessitates more runs per factor but yields more data. Only a few factors (<10) are used. Determine which factors have a significant impact on the response, including their interactions (fit a two-factor interaction model). If you have narrowed down the factors, consider adding a midpoint to this design to detect non-linear interactions. When no curves are detected, the midpoint can be used to find a factor setting that maximizes or minimizes response[54].

Optimization requires the most runs per factor, but provides the most information. After narrowing the list of known important factors (<6) whose optimum likelihood is in the area being tested, optimization is used. Can be used to find factor settings that maximize or minimize the response of the three design of experiments options, each of which includes three methods that can be used, namely factorial/response surface, mixture, and combined[54].

3.2.1 Factorial design

Factorial design is a method of modeling the relationship between the response variable and one or more independent variables using regression equations. The most common type of design for process improvement is factorial. Factorials are used in research to examine the effects of various conditions on the study's results, as well as the interactions between them. Factors, levels, and effects are all part of the factorial design. The amount of the independent variable that will affect the result output or the dependent variable is defined as a factor. The factors are classified as quantitative (numerical factors, such as a concentration of 1% or 2%) and qualitative (non-numerical factors). Quality (material's quality, for example). A factor's level is defined as its value or constant. Effects are changes in response caused by variations at the factor level. Responses are defined as the nature or outcomes of an experiment that can be quantified[55].

Chapter Four

Experimental Part

4.1 Introduction

This chapter explains the procedure preparation and characterization of Alumina and Magnesia powder, preparation the samples for mechanical and physical properties, preparation the samples for digital image correlation (DIC), crack opening displacement, fracture toughness measurement, and making an optimization model for the optimal preparation conditions of Alumina-Magnesia powder.

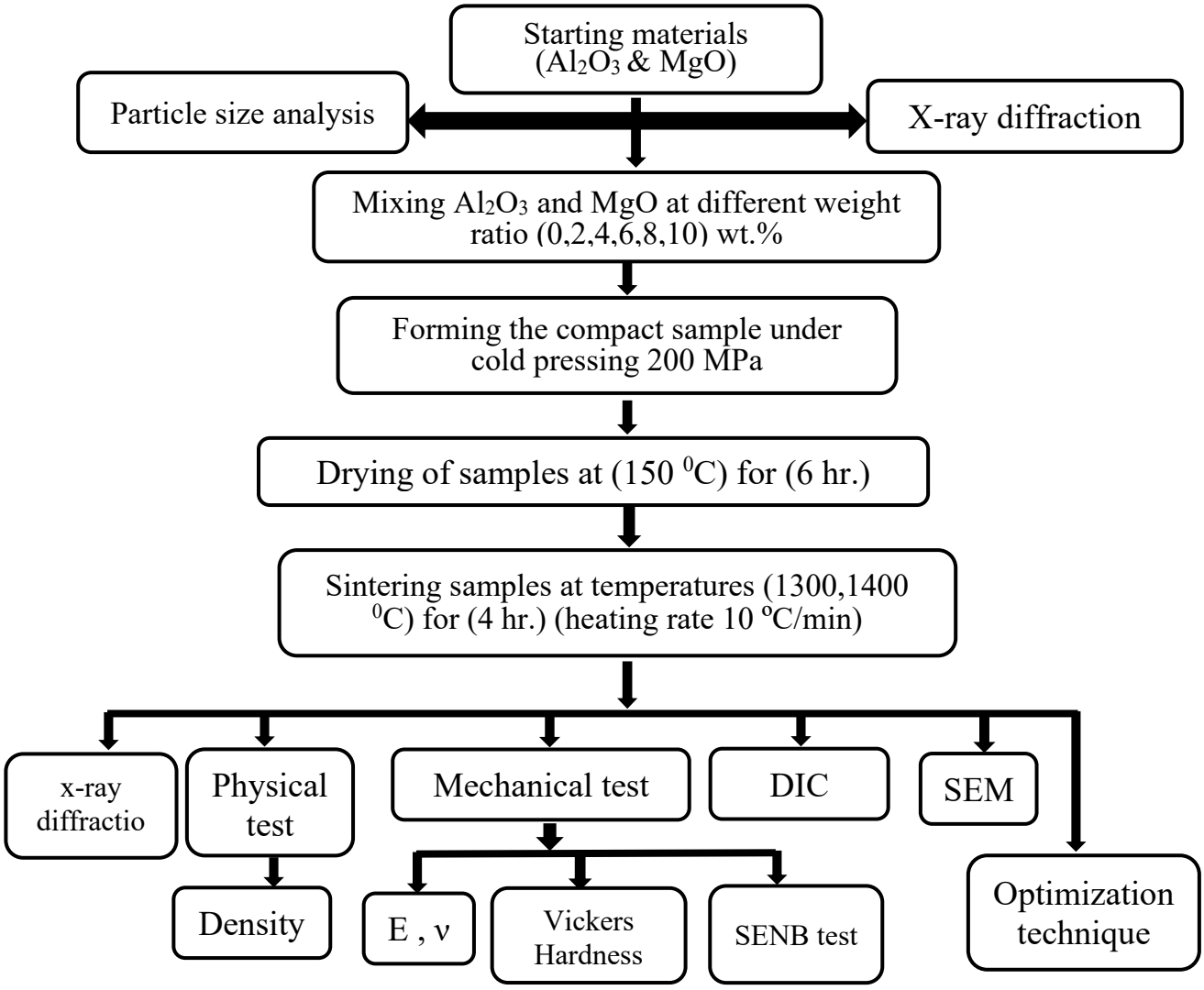

Figure (4.1): Steps to prepare (Al_2O_3-MgO) specimen.

4.2 Starting Materials

The starting components, alumina and magnesia, were subjected to an X-ray examination to determine the composition of the phases. Next, the main size of the powdered particle size was established by measuring the alumina and magnesia particle sizes. Alumina powder with particle sizes of 58.5µm were ground in planetary ball miller (SFM-1 Desk-Top Planetary Ball Miller) showing in figure (4.2) to get a finer particle size that used in the sample preparation of ceramic specimen. The alumina was milled with (0,2,4,6,8,10) wt% magnesia powder separately by ball milling mixer for 4 hrs, (with using pure Al_2O_3 ball as a milling media). Table (4.1) shows the used powders specifications.

Table (4.1): specifications of used powders.

Material	Producer	Purity %	Particle Size µm
Al_2O_3	Central Drug House	99	4.7
MgO	HiMedia Laboratories	98-100.5	4.2

Figure (4.2): SFM-1 planetary Ball Miller.

4.2.1 XRD Analysis

As shown in figure (4.3) in this study, the raw materials (alumina and magnesia) were scanned at room temperature by x-ray diffraction (Shimadzo 6000) at the University of Babylon's College of Materials Engineering's Ceramic Engineering and Building Material Department, using Cu-ka radiation (λ=1.5405 A^{o}) and a scanning speed of 50/min.

Figure (4.3): X-ray diffractometer (XRD) device.

4.2.2 Particle Size Analysis

At the University of Babylon / College of Materials / Ceramic and Building Material Department, the particle size analysis for the starting materials (alumina and magnesia) was performed using a laser partial size analyzer (Bettersize2000) equipment as illustrated in figure (4.4).

Figure (4.4): Laser particle size analyzer (Bettersize 2000).

4.3 Specimen Preparation

2.0wt% polyvinyl alcohol binder (PVA) was mixed with mixtures of Al_2O_3 and MgO. Dense samples were produced by uniaxially pressing under 200 MPa using stainless steel die. The samples were then dried for 6 hrs in 150ºC and left for 24 hrs at room temperature and presureless sintering were conducted at 1300, 1400ºC for 4 hrs at heating rate 10 ºC/min in the programmable furnace.

Two types of specimens were made with every MgO adding ratio, the rectangular shape for SENB test with dimension (50*6*4 mm) Figure (4.5 a), the cylindrical shape with different dimensions, for a physical tests (Ø=20mm, h=30 mm), for Vicker's hardness test and SEM observation (Ø=20,10 mm with low height), figure (4.5 b).

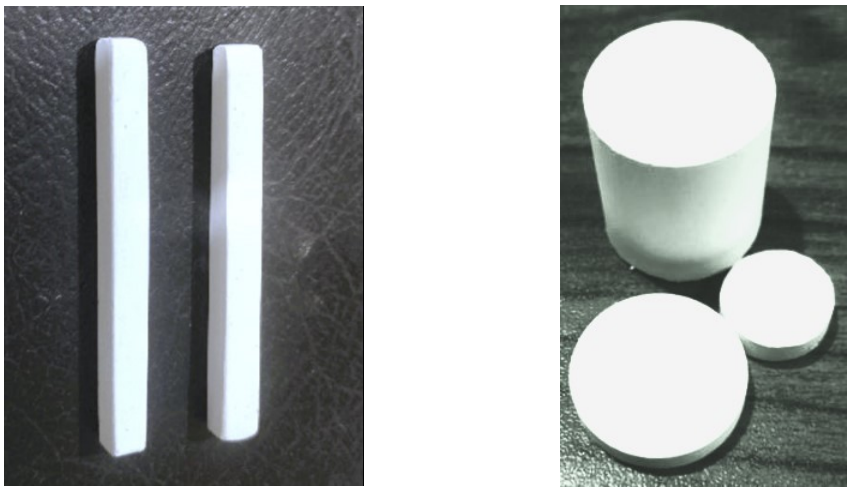

(a) **(b)**

Figure (4.5): testing specimens (a) rectangular, (b) cylindrical.

4.4 Bulk Density Measurements

Apparent Porosity and bulk density measurements of the sintered specimen was measured in accordance with ASTM C 20. Below is a list of this method's steps[56]:

1. The sample was dried at roughly 105°C. then brought to room temperature in desiccators. The dry weight (D) was calculated in (g).

2. The sample was heated for 2 hrs in a beaker filled with distilled water, with the water always keeping the sample submerged. The sample was allowed to soak for a further 12 hrs after boiling. When the examined specimen was suspended in water after impregnation, suspended mass (S) was quantified to the closest 0.01 gm.
3. The specimen was softly rolled on a damp cotton towel to remove all excess water from its surface immediately after the saturation value (S) was determined. The specimen was then weighed to determine the saturated mass (M) to the closest 0.01g.

Equations (4-1), (4-2), provide definition for the bulk density (ρ), Apparent Porosity(P):

$$\boldsymbol{\rho} = \frac{\mathbf{D}}{\mathbf{M-S}} \qquad \ldots\ldots\ldots\ldots\ldots\ldots (4\text{-}1)$$

$$\mathbf{P}\% = \frac{\mathbf{M-D}}{\mathbf{M-S}} * 100\% \qquad \ldots\ldots\ldots\ldots (4\text{-}2)$$

4.5 Calculation of mechanical properties

4.5.1 Young's Modulus and Poisson's Ratio (E, ν)

Young's modulus and Poisson's ratio of materials were calculated for a specimens with dimension (Ø=20, h=30) using the ultrasonic device (CSI type CCT-4, Department of Polymer Engineering and Petrochemical Industries, College of Materials, University of Babylon) utilizing equations (4.2) and (4.3)[57]:

$$\boldsymbol{\nu} = \frac{\mathbf{1-2}\left[\frac{C_s}{C_l}\right]^2}{\mathbf{2-2}\left[\frac{C_s}{C_l}\right]^2} \qquad \ldots\ldots\ldots\ldots\ldots (4\text{-}2)$$

$$\mathbf{E} = \mathbf{2}\boldsymbol{\rho} C_s^2(\mathbf{1}+\boldsymbol{\nu}) \qquad \ldots\ldots\ldots\ldots\ldots (4\text{-}3)$$

Where: C_l is speed of sound of longitudinal; C_s is speed of sound of shear, ρ density of the specimen, E Young's modulus and ν Poisson's ratio.

4.5.2 Vickers's Microhardness

Steel dies were used to create disc specimens with dimensions of 10 mm in diameter and 3 mm in height. To conduct the test, a digital micro-Vickers was employed.

A hardness tester, model TH-717, was used in accordance with ASTM standard E384-17 by applying 1 kg and letting it sit for 10 seconds[58].

4.5.3 Fracture Toughness (KIC)

The fracture toughness of Alumina and Alumina mixed with MgO was determined using the single edge notched beam technique and the equation from ASTM C 1421. (4.4)[33]:

$$KIC = g\left[\frac{P_{max}\ S_o\ 10^{-6}}{BW^{3/2}}\right]\left[\frac{3[a/W]^{1/2}}{2[1-a/W]^{3/2}}\right] \quad \text{..... (4-4)}$$

This equation for three-point flexure with $5 \leq \frac{a}{w} \leq 10$ and $\frac{a}{w} = 0.2 - 0.3$

Where:

KIC = fracture toughness (MPa . $\sqrt{m}$).

P_{max}=maximum force (N)

S_o = span between support (m)

B= width of specimen (m)

W= height of specimen (m)

a=crack length (m)

g= the coefficients for g are depend on the ratio of (a/W)

$$g = g\left[\frac{a}{w}\right] = A_o + A_1(a/w) + A_2(a/w)^2 + A_3(a/w)^3 + A_4(a/w)^4 + A_5(a/w)^5$$

The value of (A_o, A_1, A_2, A_3, A_4 and A_5) determined from table in ASTM 1421.

4.6 Digital Image Correlation Test

Figure (4.6 a) shows the application of black paint (vinyl acetate/ethylene VAE) on the specimen surface. The speckle pattern must be non-repetitive, isotropic, and contrasty enough for the program to recognize and compare the picture before and after deformation. Figure (4.6 b) depicts a typical speckle pattern on an item.

GOM (Gesellschaft für Optische Mebtechnik) is a German company's DIC calculation software. This computation method begins with a reference image taken prior to loading, which is then compared to a sequence of images obtained throughout the loading time. It is recommended that the color value of the photographs stay constant before and after deformation. First, the picture is divided into a number of subsets, and then a deformation or displacement distribution map is constructed by searching for the corresponding subsets following deformation based on the assumptions.

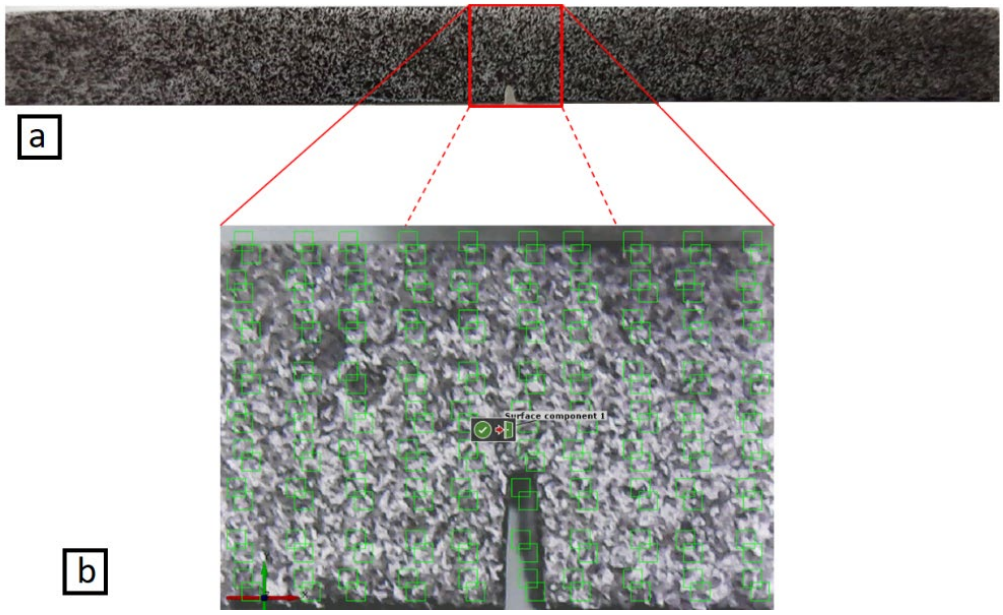

Figure (4. 6): (a) Speckles of black paint, (b) subset on the sample surface[49]

4.7 Loading Setup and Test Procedure

As shown in figure (4.7), specimens were subjected to the load microcomputer controlled electronic universal testing machine (WDW-5E in polymer Department/ Engineering materials/ University of Babylon). This testing machine has a loading capacity of 5 kN and the loading rate is very low, resulting in a displacement not exceeding 0.01 mm/min. The camera location was adjusted to keep the lens as parallel to the specimen surface as feasible, and the focal length was also adjusted to ensure a good image.

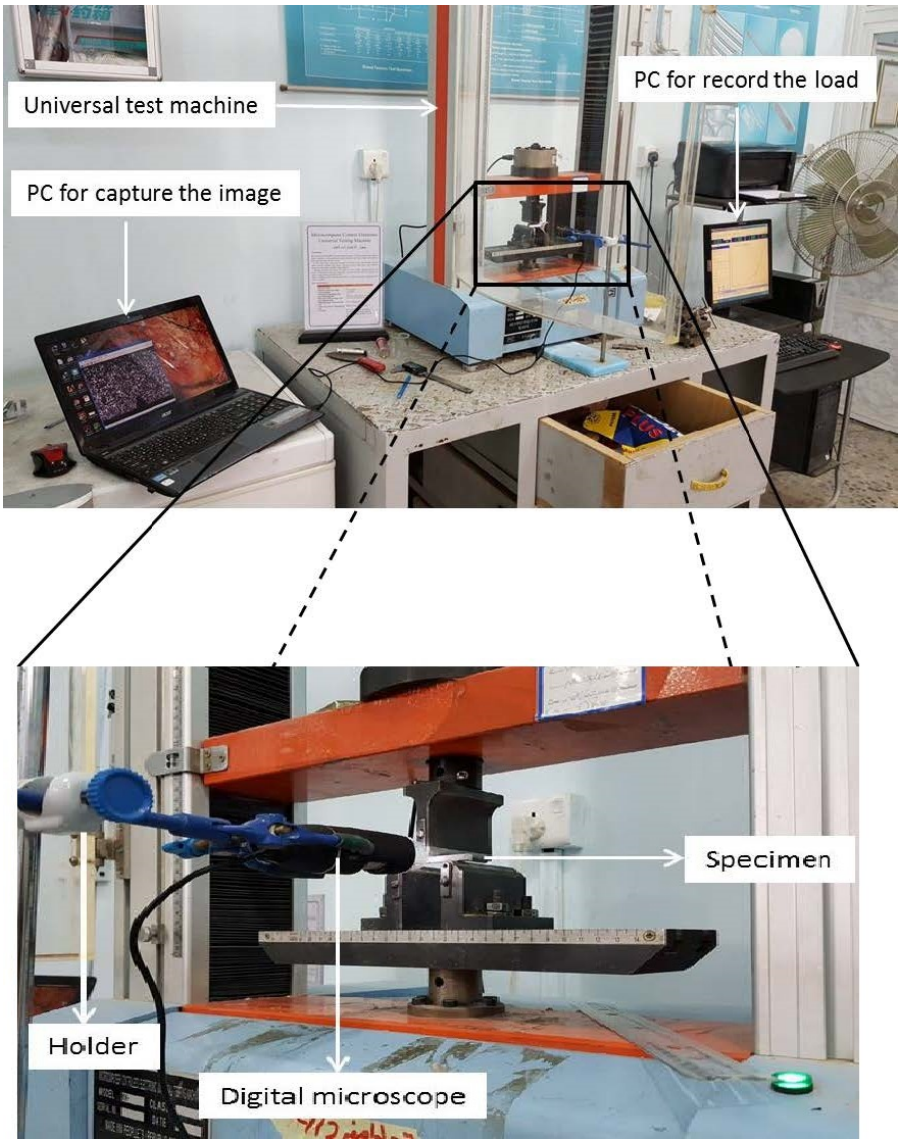

Figure (4.7): Loading Setup

4.8 Crack Propagation and Opening Using DIC

DIC (GOM) was used to investigate crack propagation and opening. After executing the application, the photos were loaded into GOM software for examination, and the cracking was observed as shown below:

4.8.1 Measurement of the Crack Opening Displacement

Figure (4.8) shows the position of the crack mouth and the displacement of the crack tip opening. The crack opening displacement (CMOD and CTOD) may be measured by DIC utilizing line profile horizontal displacement. The correlation algorithm calculates where each sub-pixel in the imaging region is located. Displacement contours may be used to simply compute horizontal (axial) displacement. A discontinuity (crack) in the material can be seen as a dramatic jump in the displacement values.

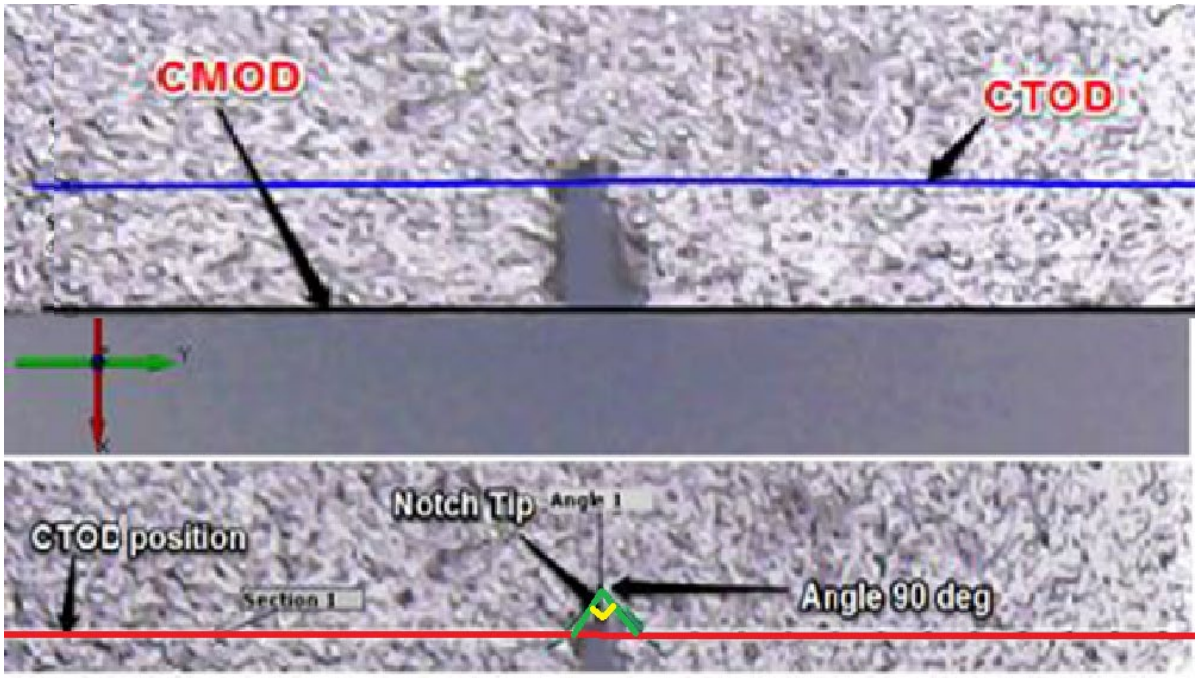

Figure (4.8): Position of CMOD and CTOD[49]

4.8.2 Detection Crack Propagation Using DIC

The region of interesting (ROI) above the notch tip is considered while evaluating fracture propagation. Taking the horizontal strain (ε_{xx}) to show the strain map, which leads to identifying fracture propagation and determining crack site by taking the strain on line profile, as shown in the figure (4.9).

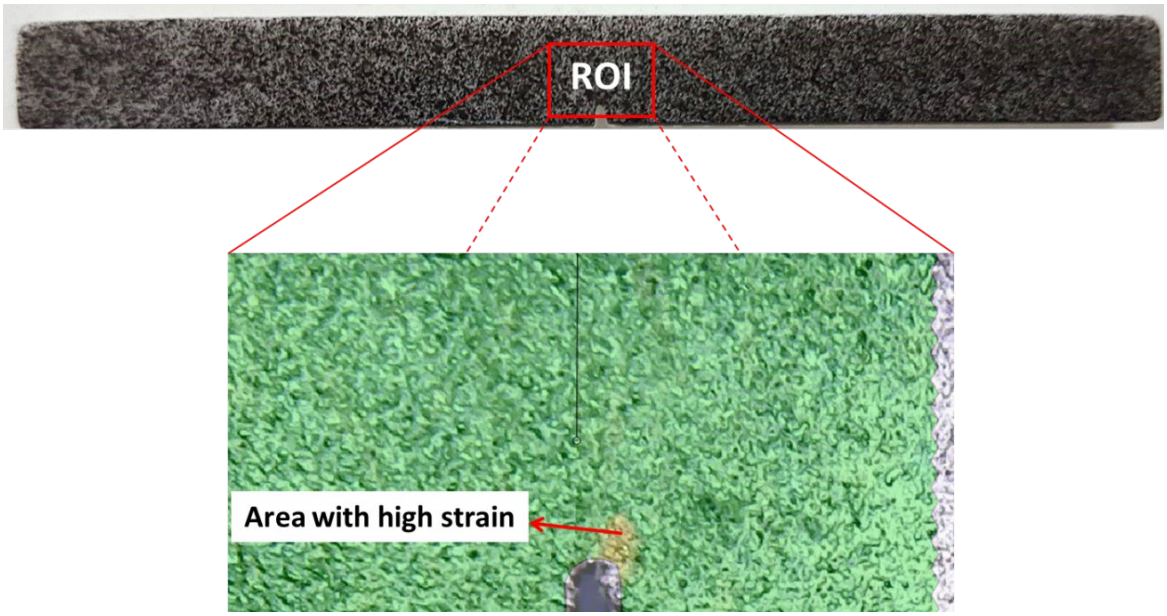

Figure (4.9): Shows high strain area which refer to crack propagation[49]

4.9 Optimization Model

"Design Expert" program was using to made an optimization model for production processes by made a desirability comparison between the results and the effect of the introduction (dependent) variable (wt.% MgO, Temperature) on the results (independent variable) (Density, HV), then the program predicts the optimum percent of Magnesia and the sintering temperature that gave the optimum result.

Chapter Five

Results & Discussion

5.1 Introduction

This chapter displays the results of the experimental work as well as the discussion of these results. It is divided into three sections: the first discusses the results and discussion of the experimental work, the second demonstrates the results of the Digital Image Correlation technique of crack propagation and opening for Alumina sample and Alumina doped with MgO, and the third reveals the Optimization model of the results using Design Expert program.

5.2 Characterization of the Starting Materials

5.2. 1 X-Ray Diffraction

X-ray diffraction technique was used to identify the phases that present in the materials; figure (5.1) shows the result of x-ray diffraction analysis of Alumina that matches the (96-901-2251) reference code of Alumina , figure (5.2) shows the result of x-ray diffraction analysis of Magnesia that matches the (96-900-6750) reference code of Magnesia, figures (5.3), (5.4) show the result of x-ray diffraction analysis of powder of ground produced specimens sintered at 1400^{o}C with (4, 10 wt.% MgO) that have an Alumina and Spinal (Al_2MgO_4) matches the (96-900-9672) reference code of Alumina, and (96-900-2847), (96-900-2848) reference code of spinal.

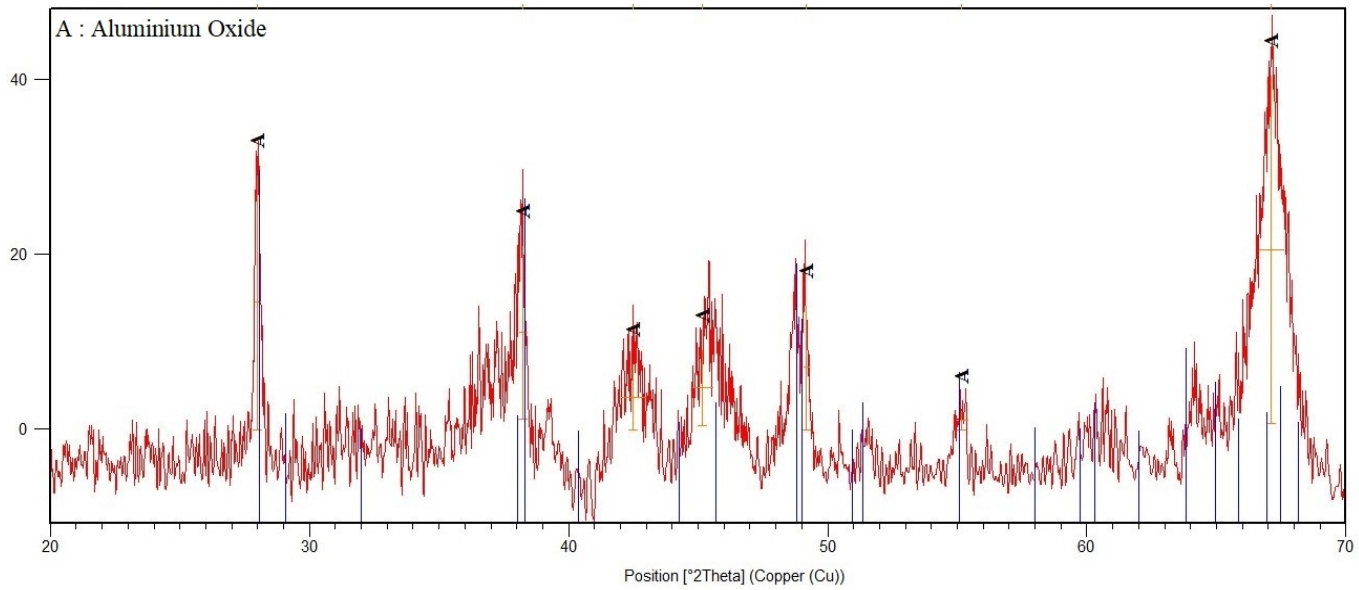

Figure (5.1): XRD Al_2O_3 sample

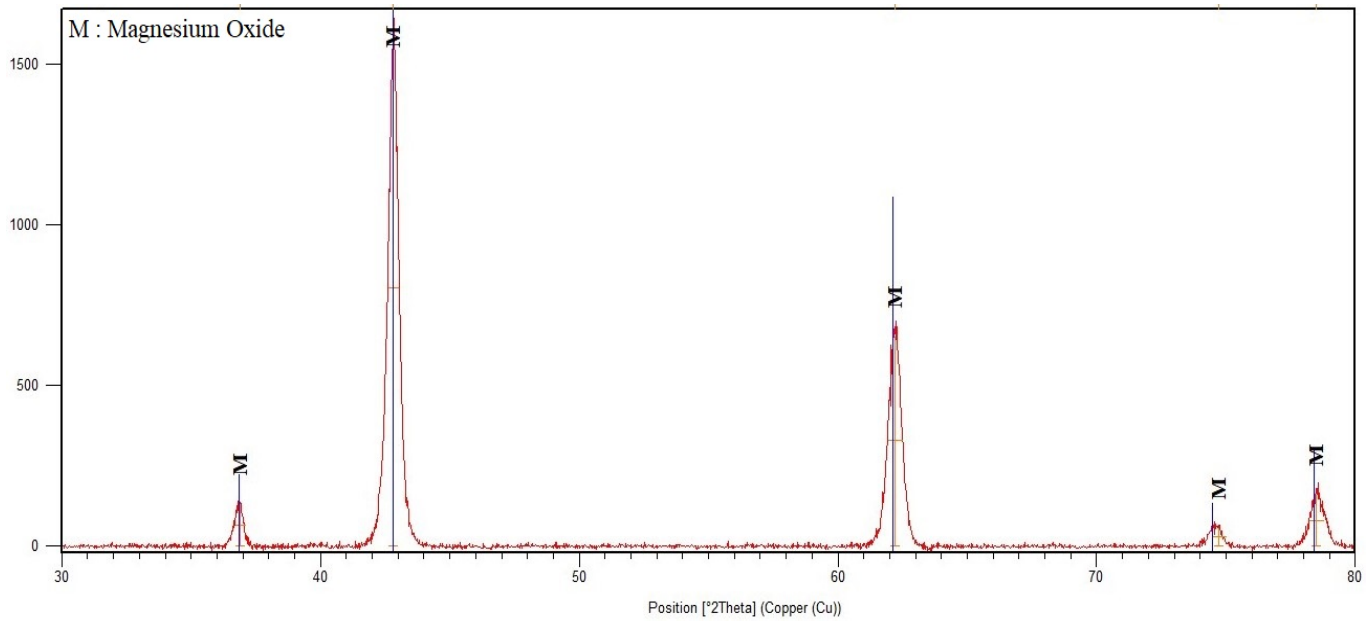

Figure (5.2): XRD MgO sample

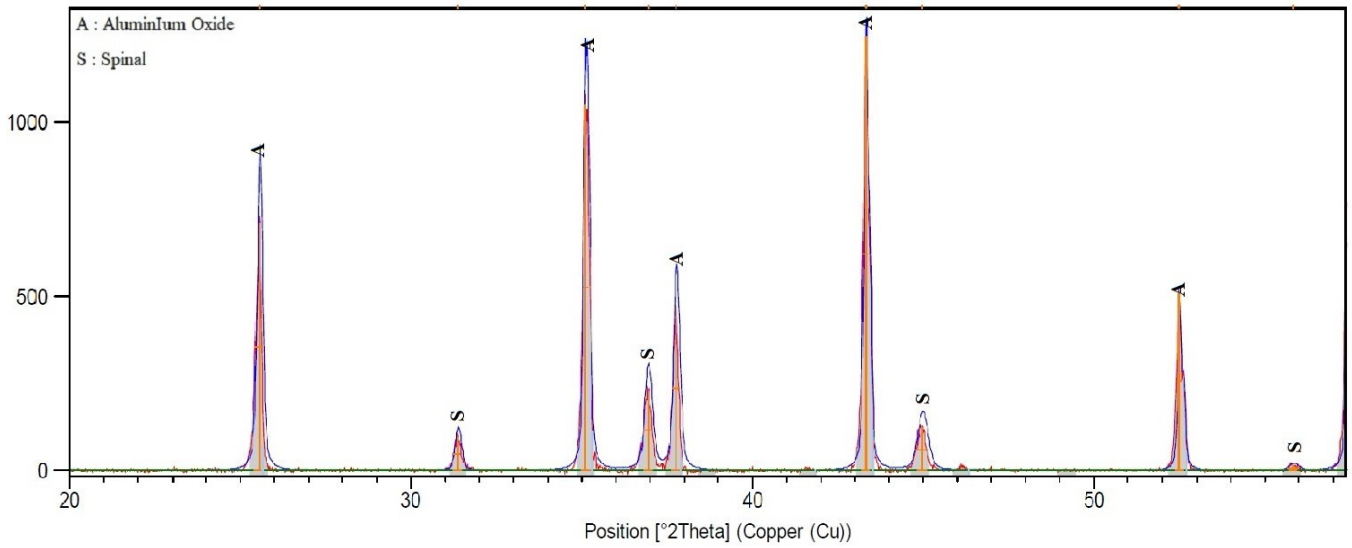

Figure (5.3): XRD of product sample has (4 wt.% MgO), sintered at 1400°C

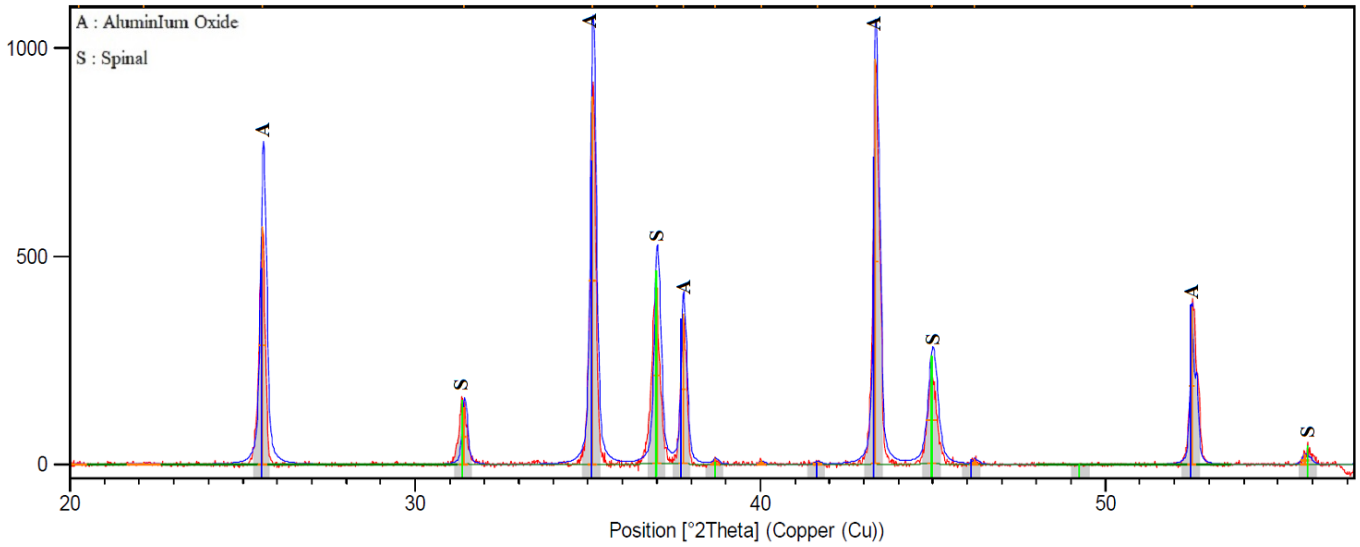

Figure (5.4): XRD of product sample has (10 wt.% MgO), sintered at 1400°C

5.2. 2 Particle Size Analysis

Figures (5.5) and (5.6) depict the particle size distribution analysis of the Alumina and Magnesia starting material powders after 3 hours of milling (just for Alumina). Alumina particles ranged from 0.9 to 40 m. (0.857, 4.677, and 40.57, respectively) for D10, D50, and D90, while Magnesia particles ranged from 0.9 to 20 m. (0.889, 4.151, and 19.67, respectively) for D10, D50, and D90.

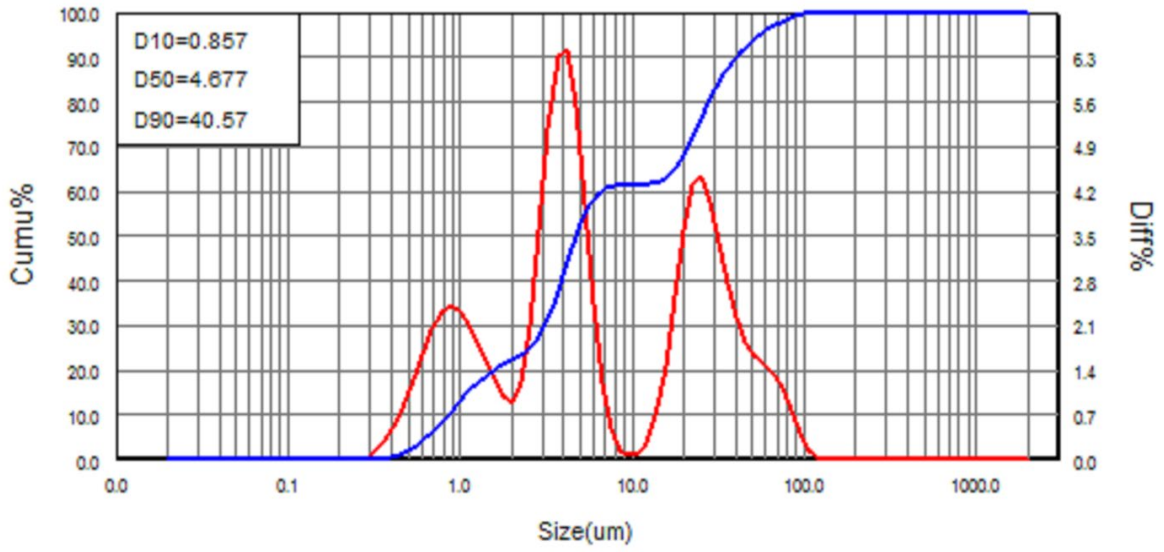

Figure (5.5): P.S distribution of Al_2O_3 powder

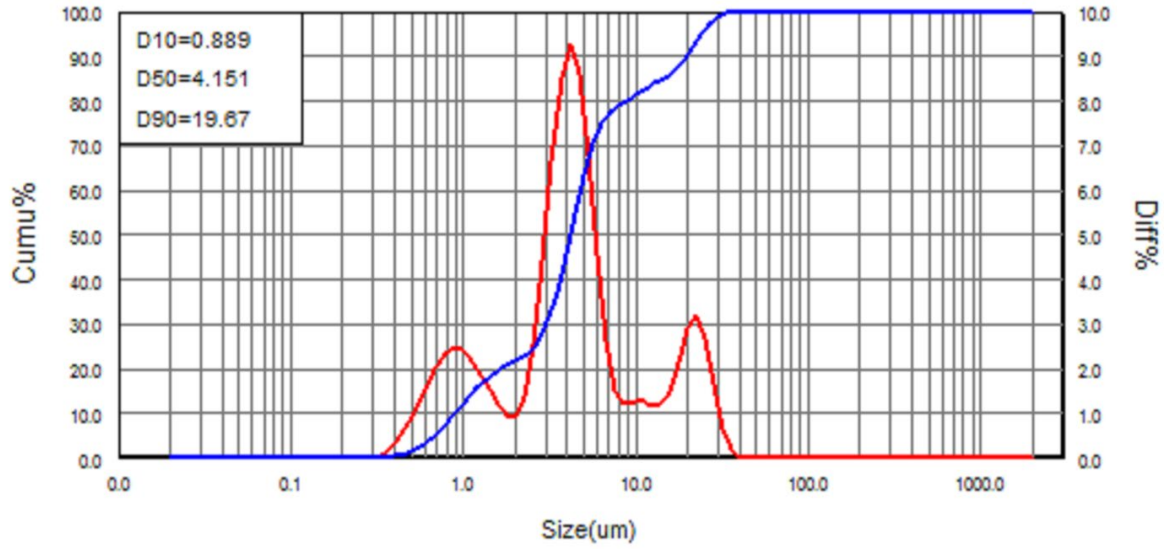

Figure (5.6): P.S distribution of MgO powder

5.3 Experimental Results

5.3. 1 The physical Properties (Apparent Porosity and Bulk Density)

The apparent porosity and bulk density are a factors that influence the mechanical and physical properties of ceramic materials. Figures (5.7), (5.8)

depicts the effect of MgO content on compact sample density and porosity. When MgO was added, the apparent porosity decreased until (6wt.% MgO) then increase by formation an excess amount of spinal that suppress alumina grain growth, causing inability to fill the porosity consequently. The bulk density decreased by adding MgO, its highest at pure Alumina (1.935 g/cm^3) and then gradually decreases as the amount of MgO increases, the smaller density of the spinal compared with the alumina and the increment in the porosity are the reasons of density decreasing.

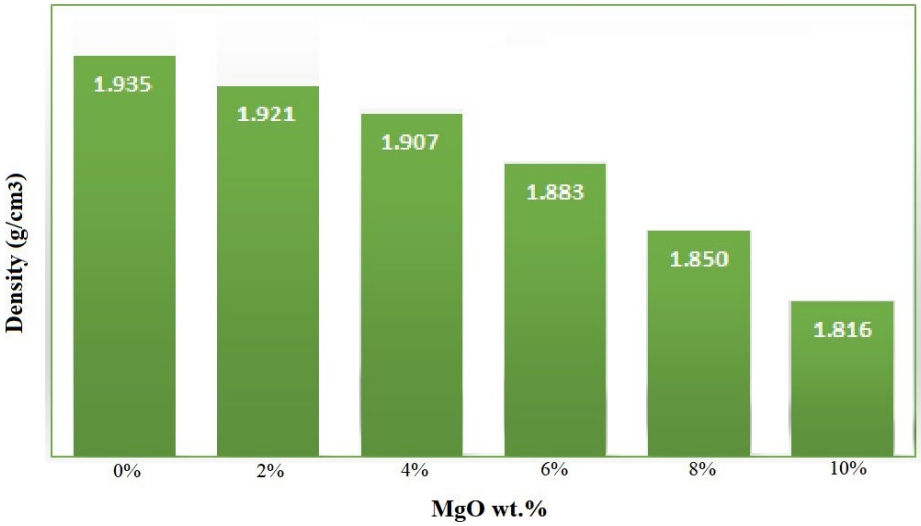

Figure (5.7): The effect of MgO on density for specimens sintered at 1400°C

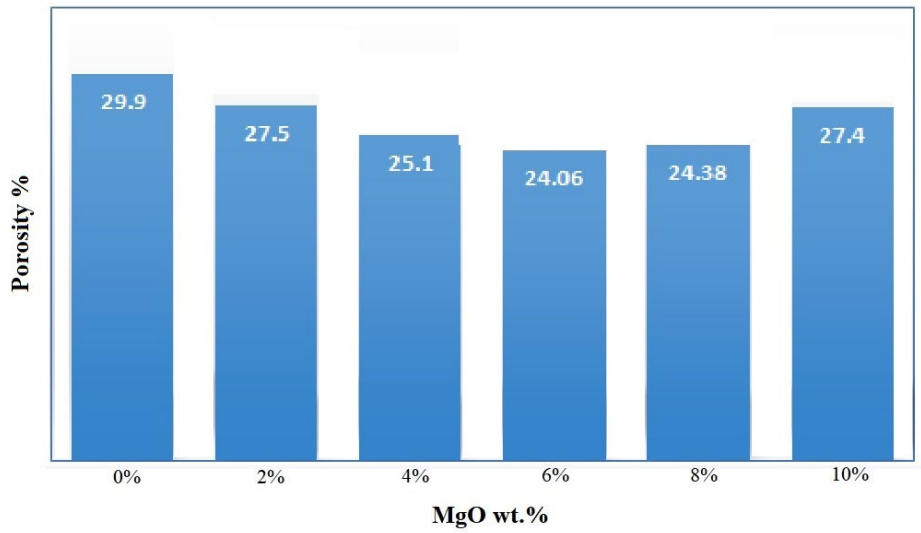

Figure (5.8): The effect of MgO on porosity for specimens sintered at 1400°C

5.3. 2 Microstructural Observation

By using a SEM instrument to observe the microstructure, the figure (5.9) shows the effect of the MgO additive by refining the grain size. The images (a), (b) represent the pure Al_2O_3 and Al_2O_3/4wt% MgO in 500x magnification respectively, while the images (c), (d) represent the pure Al_2O_3 and Al_2O_3/4wt% MgO in 1000x magnification respectively.

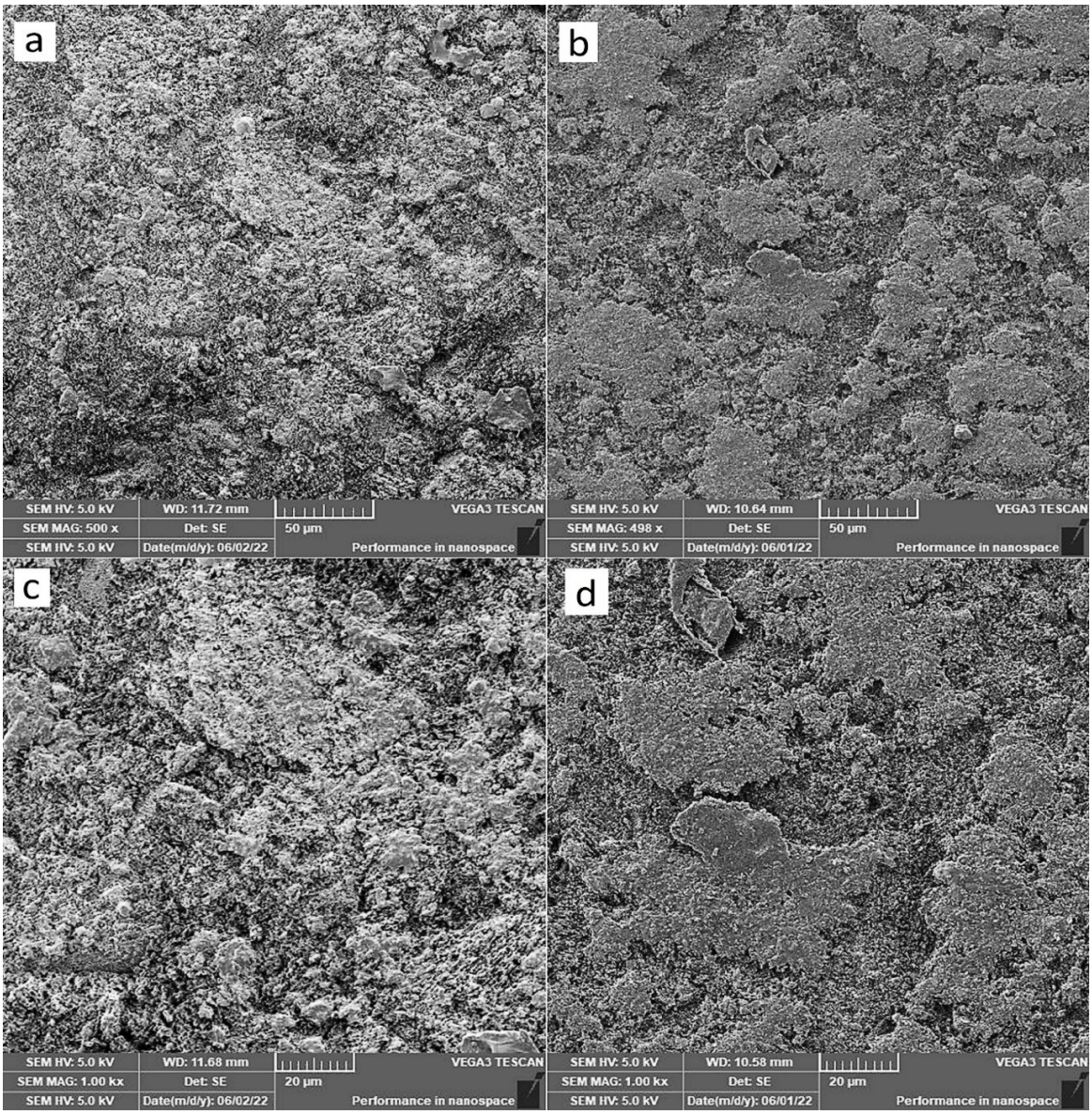

Figure (5.9): The effect of MgO on density for specimens sintered at 1400°C a) Al_2O_3 in 500x, b) Al_2O_3/4wt% MgO in 500x, c) Al_2O_3 in 1000x, d) Al_2O_3/4wt% MgO in 1000x

5.3. 3 Mechanical Properties

5.3.2.1 Young's Modulus and Poisson's Ratio (E,ν)

The ultrasonic method results for determining (E, ν) are shown in the table (5.1). The increase in Young's modules and Poisson's ratio was related to the effect of MgO sinterability, which inhibited grain growth and enhanced sample's properties[59], [60].

Table (5.1): Young's modulus and Poisson's ratio of specimen

MgO wt. (%)	E (Gpa)	ν
0	29	0.225
2	32	0.224
4	36	0.227
6	40	0.228
8	42	0.230
10	46	0.234

5.3.2.2 Fracture Toughness and Vickers' Microhardness

The results of fracture stress, fracture toughness test using SENB method that calculated according to ASTM C 1421[33], and Vickers' Microhardness test are shown in the table 5-2.

Table (5.2): fracture stress, Fracture toughness & Vickers' Microhardness test results

MgO wt. (%)	σ (MPa)	KIC (MPa. √ m)	HV
0	0.270	0.713	21.98
2	0.322	0.857	23.64
4	0.478	1.264	30.68
6	0.240	0.648	27.57
8	0.273	0.699	28.05
10	0.319	0.831	29.66

The increase in fracture toughness and microhardness in Alumina specimen with MgO addition can be attributed to the effect of MgO as a sintering aid, which suppresses Alumina grain growth[61], after 4wt% the mechanical properties will decrease when the MgO content increment. This attributed to spinal formation in excess amount, and because of the low mechanical properties of the spinal compared with Alumina[22].

5.4 Digital Image Correlation (DIC)

5.4. 1 Crack Propagation of Samples

Figures (5.11) show the results of DIC in pure Alumina, (5.12), (5.13), (5.14), and (5.15), (5.16) respectively, show the results of DIC in Alumina/Magnesia specimens with (2, 4, 6, 8, and10 wt.% MgO) sintered at 1400°C to determine crack propagation with time. These figures depict the change in strain mapping around the notch over time for various specimens. Each figure contains six images. Image (a) shows an undeformed specimen (before loading), while image (b) shows no change in strain mapping near the notch tip, whereas image (c) shows a change in strain mapping near the notch tip, indicating a stress concentration at the notch tip. A critical load and crack initiate occurred, as shown in the illustration (c). Following that, the specimen's bearing capacity is lost, and the load rapidly decreases as the crack propagates (d), (e). Next the crack will rapidly grow in all cross-section area (f).

In pure Alumina specimens, the crack propagates in high speed after initiation comparing with Alumina/Magnesia specimens - that have more resistance to crack propagation -.

Figure (5.8) shows the relation between added Magnesia percent versus the time of fracture and the fracture stress.

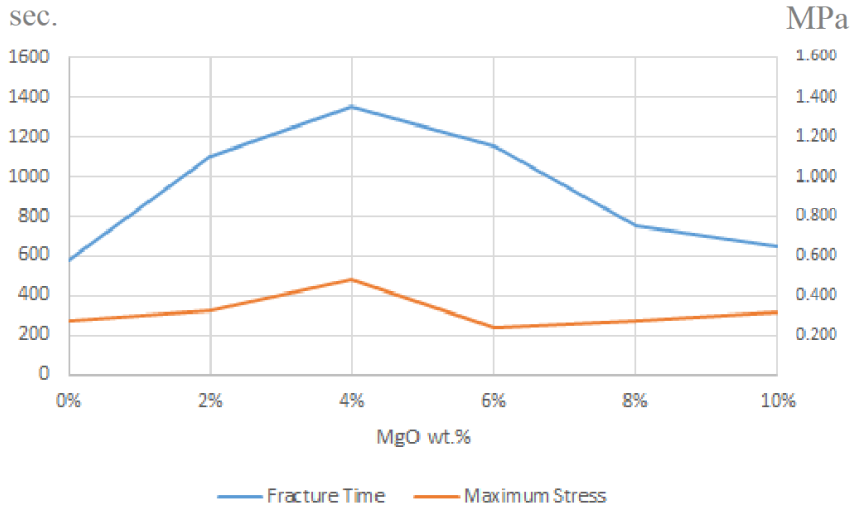

Figure (5.10) MgO percent versus time of fracture and the fracture stress

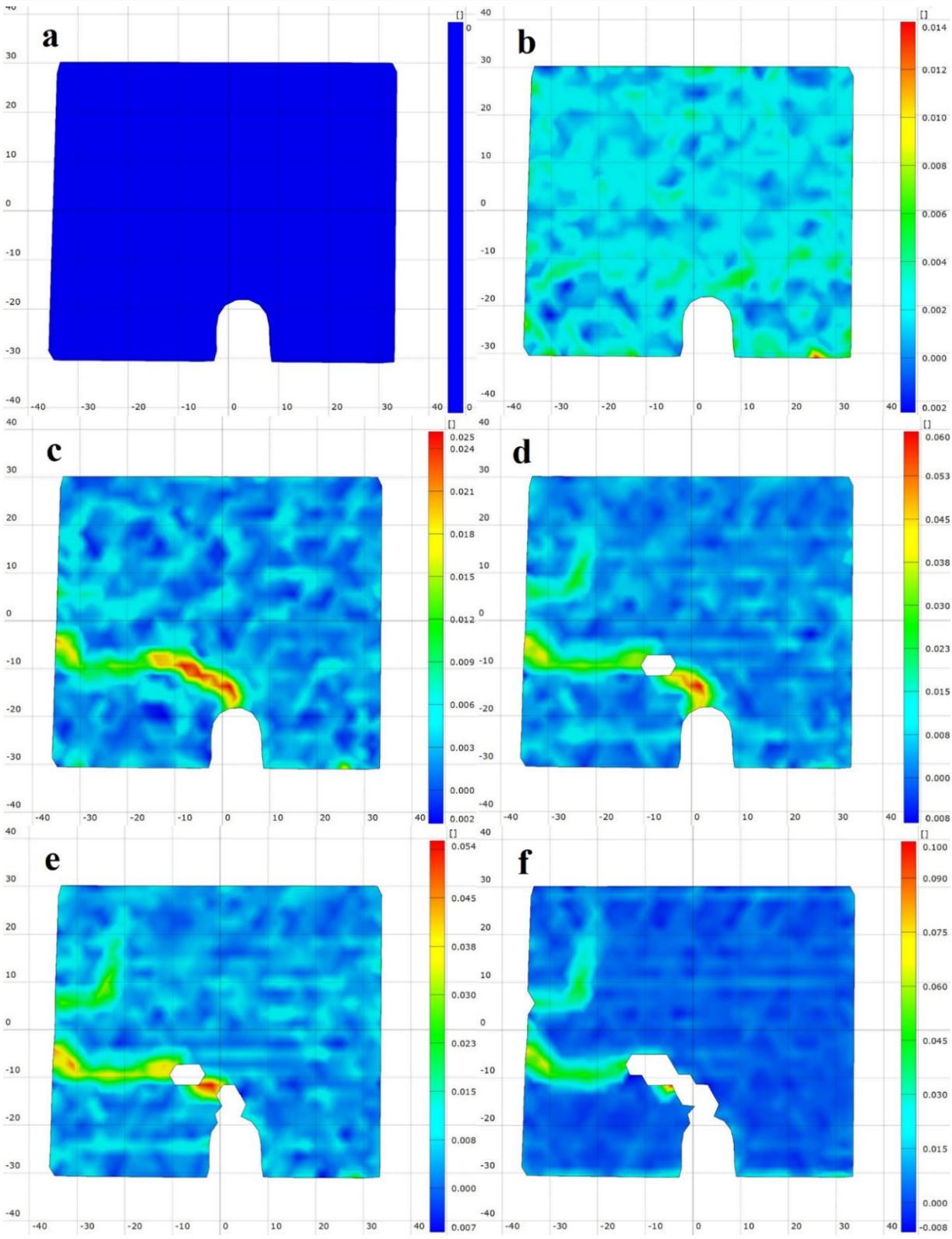

Figure (5.11) Strain maps of (Al_2O_3), sintered at 1400°C with different loads and times (a) P=0 N, t=0 s, (b) P = 7 N, t=580 s, (c) P=6 N, t=630 s, (d) P=3 N, t=700 s, (e) P=1 N, t=800 s, (f) P=0 N, t=830 s

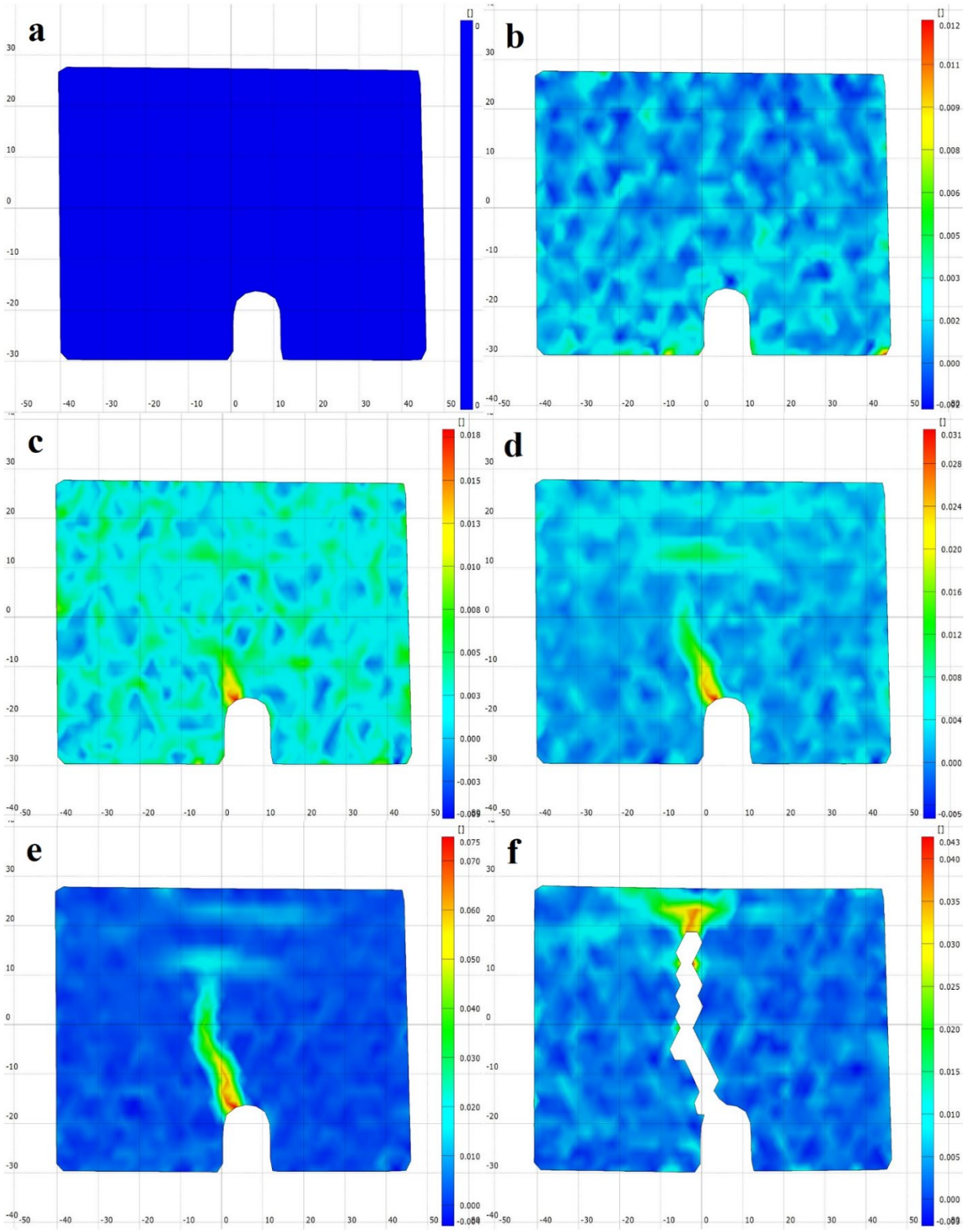

Figure (5.12) Strain maps of (Al_2O_3/2wt%MgO) , sintered at 1400°C with different loads and times (a) P=0 N, t=0 s, (b) P = 9 N, t=1100 s, (c) P=5 N, t=1200 s, (d) P=3 N, t=1220 s, (e) P=1 N, t=1230 s, (f) P=0 N, t=1250 s

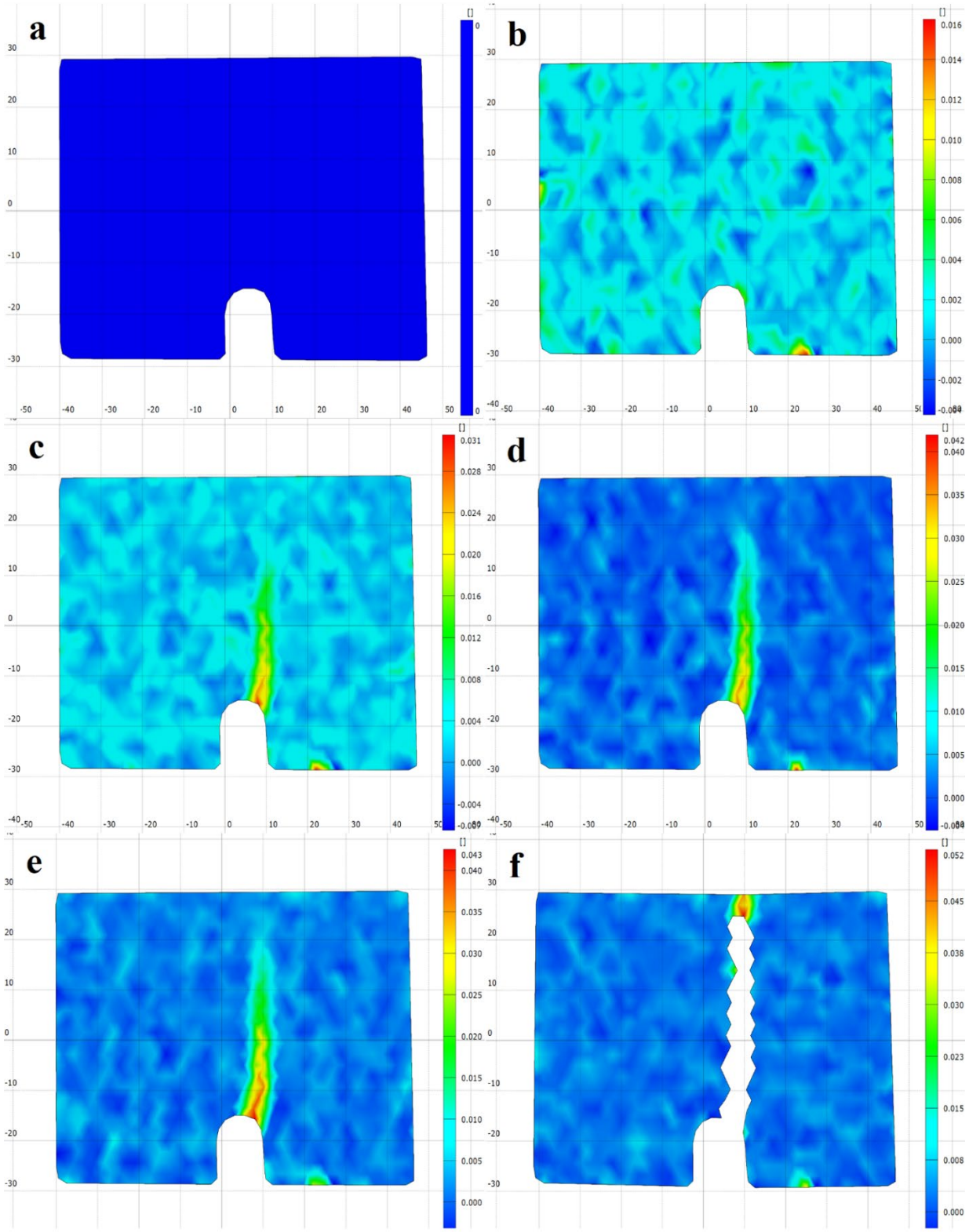

Figure (5.13) Strain maps of (Al_2O_3/4wt%MgO) , sintered at 1400°C with different loads and times (a) P=0 N, t=0 s, (b) P = 12 N, t=1350 s, (c) P=7 N, t=1500 s, (d) P=4 N, t=1600 s, (e) P=1 N, t=1650 s, (f) P=0 N, t=1675 s

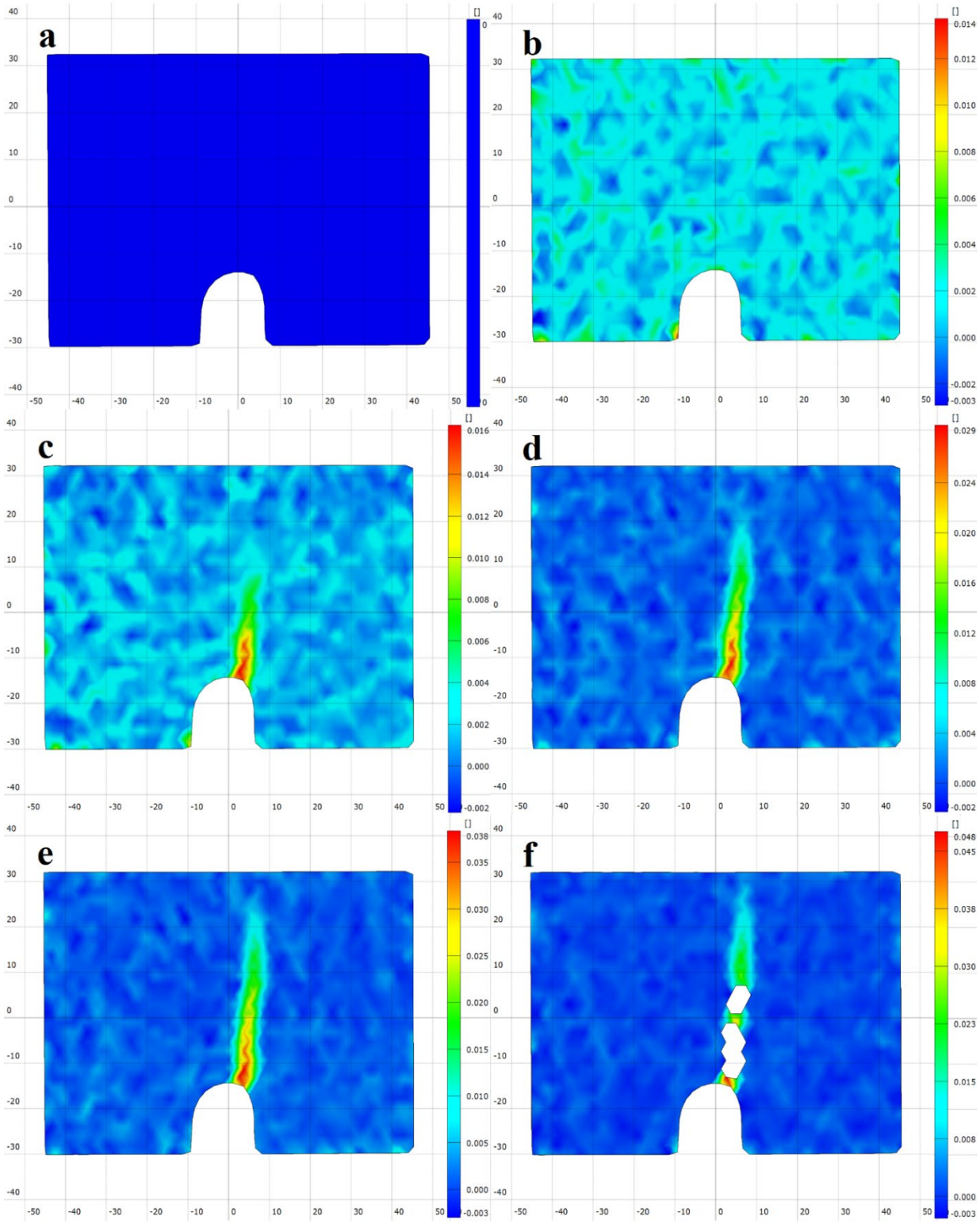

Figure (5.14) Strain maps of (Al_2O_3/6wt%MgO) , sintered at 1400°C with different loads and times (a) P=0 N, t=0 s, (b) P = 6 N, t=1150 s, (c) P=4 N, t=1300 s, (d) P=3 N, t=1375 s, (e) P=1 N, t=1450 s, (f) P=0 N, t=1500 s

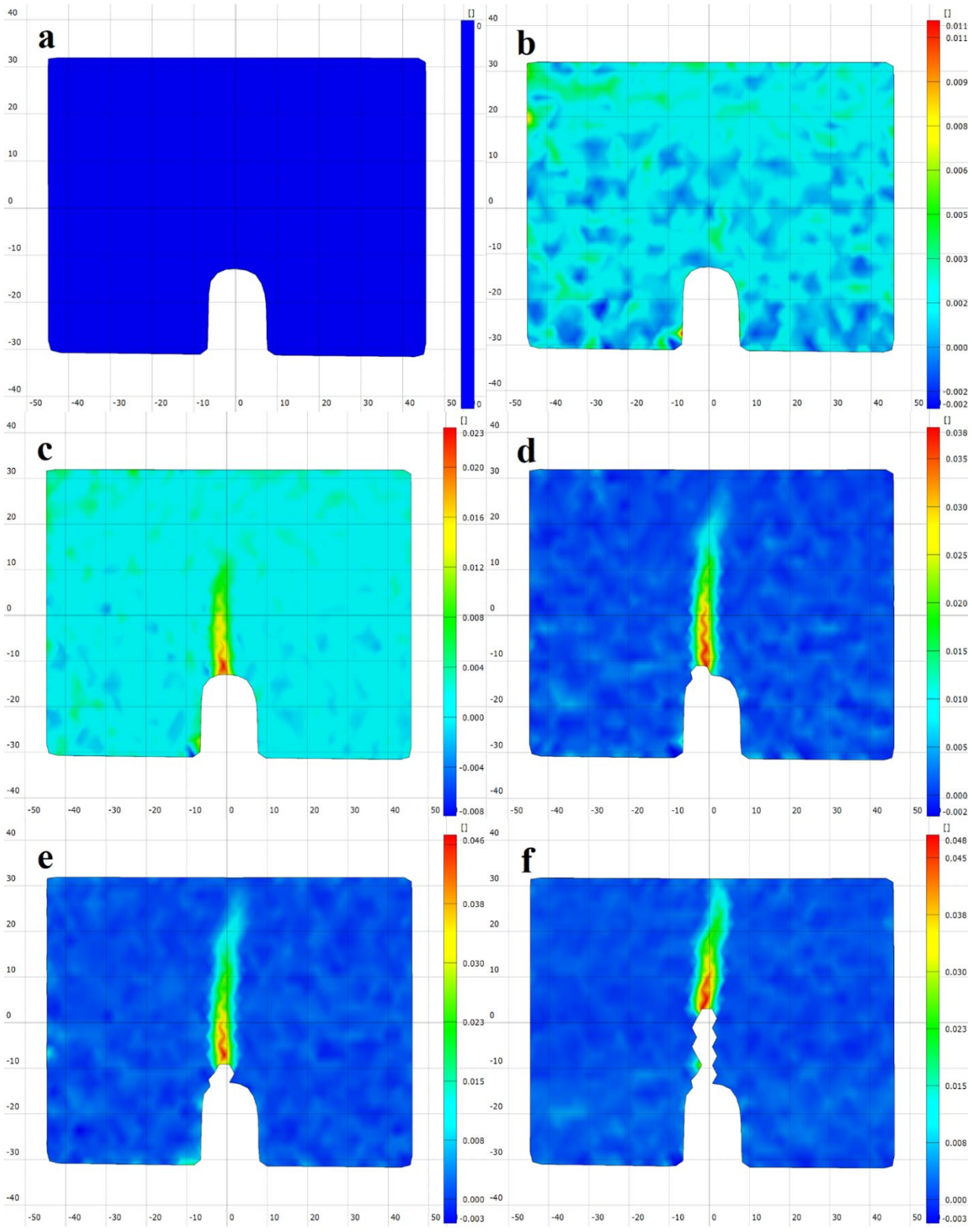

Figure (5.15) Strain maps of (Al_2O_3/8wt%MgO) , sintered at 1400°C with different loads and times (a) P=0 N, t=0 s, (b) P = 7 N, t=750 s, (c) P=3 N, t=780 s, (d) P=2 N, t=800 s, (e) P=1 N, t=825 s, (f) P=0 N, t=850 s

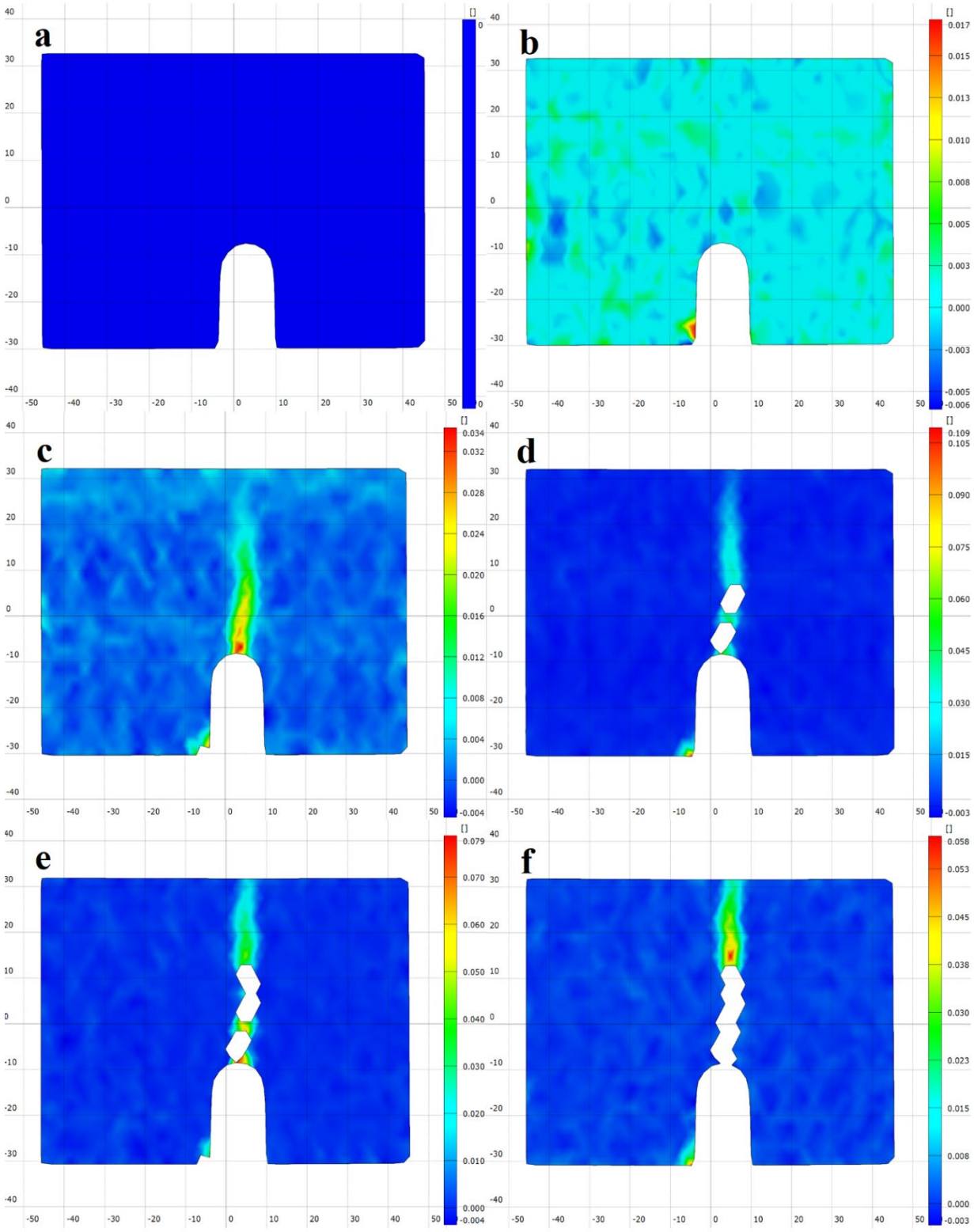

Figure (5.16) Strain maps of (Al_2O_3/10wt%MgO) , sintered at 1400°C with different loads and times (a) P=0 N, t=0 s, (b) P = 8 N, t=650 s, (c) P=4 N, t=675 s, (d) P=2 N, t=700 s, (e) P=1 N, t=725 s, (f) P=0 N, t=750 s

5.4. 2 Crack Opening of Samples

The relationship between applied force and crack opening displacement is depicted in Figures (5.17) and (5.18). (CMOD and CTOD). As shown in the diagram, the load against CMOD and CTOD curve for pure Alumina can be divided into three parts. In the beginning, the relationship was linear. The second section began. As soon as the curve deviated from linearity. The crack's opening accelerates, indicating the onset of material deterioration. The load increased in this section until the peak load reached a critical value, and the material could not go beyond this maximum loading capacity. The final stage began after the peak critical load stage, when CMOD continued to increase and the load began to decrease. CTOD and CMOD results for the specimens when add MgO show that the two curve shapes (CMOD, CTOD) differ slightly from pure Alumina curved. It was also divided into two sections. The first section was linear until it reached a peak load (maximum Load). In the second section, the tail of the curve shows the (CMOD, CTOD) increasing while the Load gradually decreasing. The difference in curve behavior is due to the toughening mechanism caused by MgO addition, which impede crack propagation, requiring more energy to propagate the crack later by refining the grain size of the Alumina.

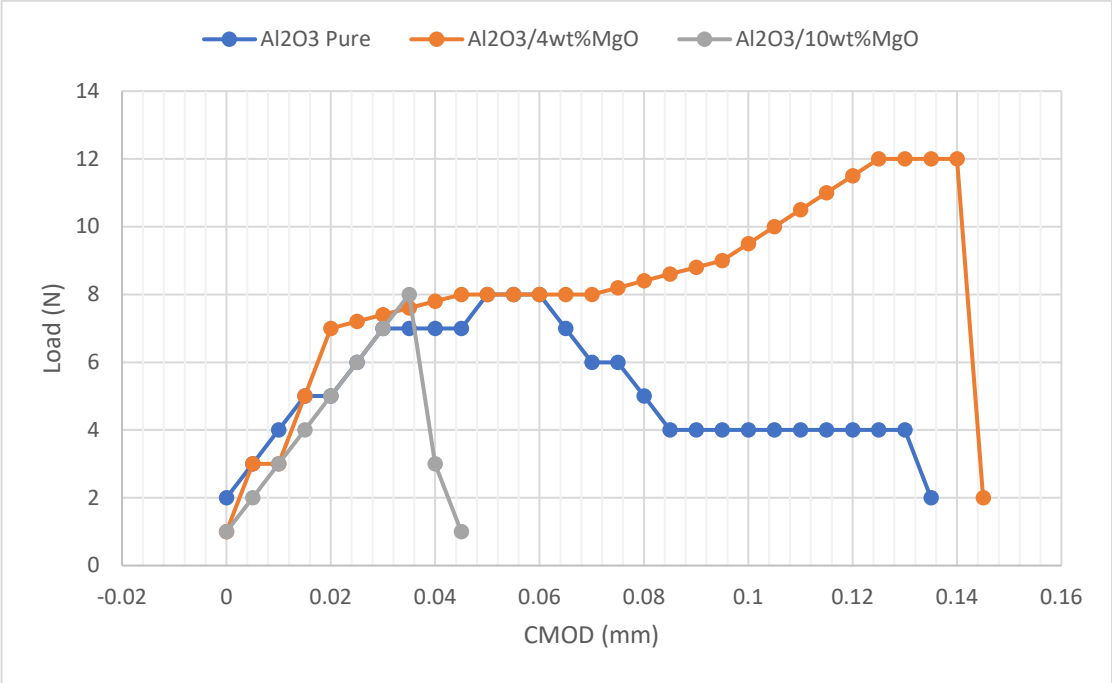

Figure (5.17) Load versus CMOD for pure Al_2O_3, Al_2O_3/4%MgO, and Al_2O_3/10%MgO, for specimens sintered at 1400°C

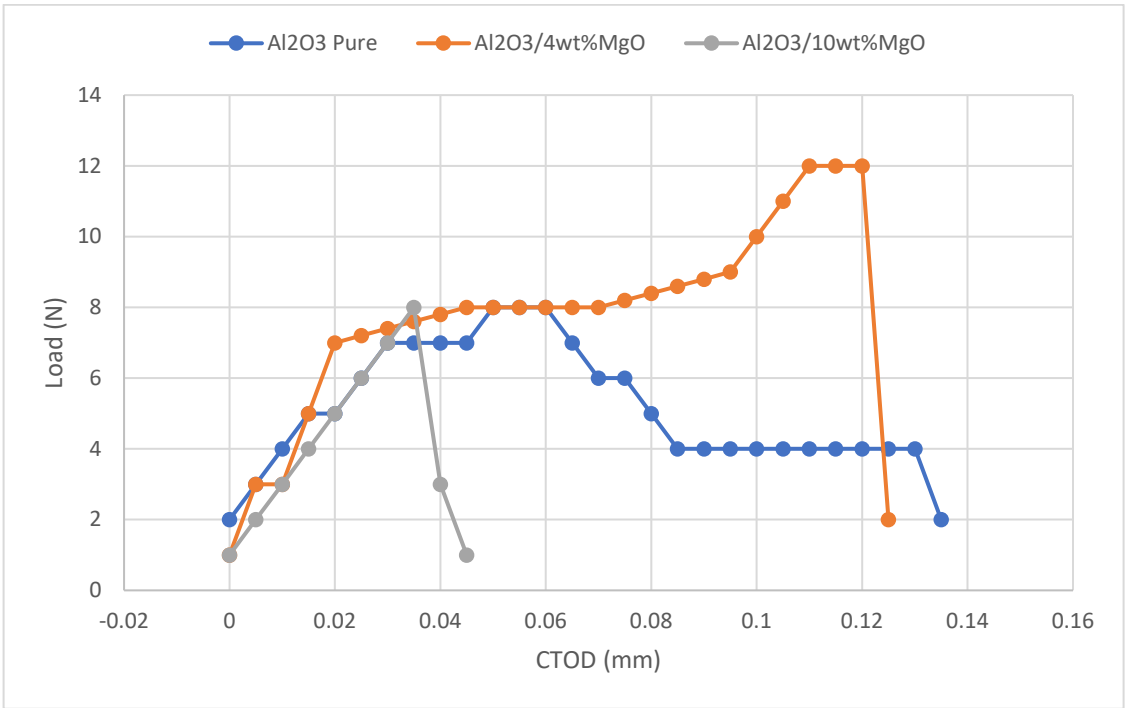

Figure (5.18) Load versus CTOD for pure Al_2O_3, Al_2O_3/4%MgO, and Al_2O_3/10%MgO, for specimens sintered at 1400°C

5.5 Optimization Method

A prediction model for physical properties (bulk density) and mechanical behavior (fracture toughness and Vickers's microhardness) was established using the factorial regression by taking these properties as a response (dependent variables) and the concentration of MgO at the range between (0 – 10 wt. %) and the heating temperature (1300,1400) °C was taken as a continuous predictor (independent variables). The result obtained by the program was as in tables (5.3), (5.4), (5.5), (5.6), (5.7), (5.8), (5.9) and figures (5.19), (5.20)

Table (5.3): Design of Experiments (DOE).

Run	Factors		Responses	
	A:MgO	B:Temperature	Density	H.V
1	0	1300	1.565	18.74
2	2	1300	1.552	21.43
3	4	1300	1.543	27.49
4	6	1300	1.518	24.36
5	8	1300	1.476	25.67
6	10	1300	1.429	26.42
7	0	1400	1.688	21.98
8	2	1400	1.678	23.64
9	4	1400	1.669	30.68
10	6	1400	1.641	27.57
11	8	1400	1.596	28.05
12	10	1400	1.55	29.66

Table (5.4): ANOVA for selected factorial model (Density).

Source	Sum of Squares	df	Mean Square	F-value	p-value	
Model	0.0736	6	0.0123	3980.41	< 0.0001	significant
A-MgO	0.0281	5	0.0056	1824.48	< 0.0001	
B-Temperature	0.0455	1	0.0455	14760.03	< 0.0001	
Residual	0.0000	5	3.083E-06			
Cor Total	0.0737	11				

Factor coding is **Coded**.

Sum of squares is **Type II Classical**

The **Model F-value** of 3980.41 implies the model is significant. There is only a 0.01% chance that an F-value this large could occur due to noise.

P-values less than 0.0500 indicate model terms are significant. In this case A, B are significant model terms. Values greater than 0.1000 indicate the model terms are not significant. If there are many insignificant model terms (not counting those required to support hierarchy), model reduction may improve your model.

Table (5.5): Fit Statistics.

Std. Dev.	0.0018	**R^2**	0.9998
Mean	1.58	**Adjusted R^2**	0.9995
C.V. %	0.1115	**Predicted R^2**	0.9988
		Adeq Precision	193.9916

The **Predicted R^2** of 0.9988 is in reasonable agreement with the **Adjusted R^2** of 0.9995; i.e. the difference is less than 0.2.

Adeq Precision measures the signal to noise ratio. A ratio greater than 4 is desirable. Your ratio of 193.992 indicates an adequate signal. This model can be used to navigate the design space.

Table (5.6): ANOVA for selected factorial model (H.V).

Source	Sum of Squares	df	Mean Square	F-value	p-value	
Model	138.59	6	23.10	199.62	< 0.0001	significant
A-MgO	113.15	5	22.63	195.58	< 0.0001	
B-Temperature	25.43	1	25.43	219.81	< 0.0001	
Residual	0.5785	5	0.1157			
Cor Total	139.16	11				

Factor coding is **Coded**.

Sum of squares is **Type II Classical**

The **Model F-value** of 199.62 implies the model is significant. There is only a 0.01% chance that an F-value this large could occur due to noise.

P-values less than 0.0500 indicate model terms are significant. In this case A, B are significant model terms. Values greater than 0.1000 indicate the model terms are not significant. If there are many insignificant model terms (not counting those required to support hierarchy), model reduction may improve your model.

Table (5.7): Fit Statistics.

Std. Dev.	0.3402	**R^2**	0.9958
Mean	25.47	**Adjusted R^2**	0.9909
C.V. %	1.34	**Predicted R^2**	0.9761
		Adeq Precision	44.7907

The **Predicted R^2** of 0.9761 is in reasonable agreement with the **Adjusted R^2** of 0.9909; i.e. the difference is less than 0.2.

Adeq Precision measures the signal to noise ratio. A ratio greater than 4 is desirable. Your ratio of 44.791 indicates an adequate signal. This model can be used to navigate the design space.

Table (5.8): Constraints.

Name	Goal	Limit		Weight		Importance
		Lower	Upper	Lower	Upper	
A:MgO	is in range	0	10	1	1	3
B:Temperature	is in range	1300	1400	1	1	3
Density	maximize	1.429	1.688	1	1	2
H.V	maximize	18.74	30.68	1	1	3

Table (5.9): Solutions for 12 combinations of categoric factor levels.

Number	MgO	Temperature	Density	H.V	Desirability	
1	**4**	**1400**	**1.668**	**30.541**	**0.961**	**Selected**
2	6	1400	1.641	27.421	0.762	
3	8	1400	1.598	28.316	0.738	
4	10	1400	1.551	29.496	0.695	
5	4	1300	1.544	27.629	0.606	
6	2	1400	1.677	23.991	0.600	
7	0	1400	1.688	21.816	0.443	
8	6	1300	1.518	24.509	0.421	
9	8	1300	1.474	25.404	0.351	
10	2	1300	1.553	21.079	0.280	
11	0	1300	1.565	18.904	0.059	

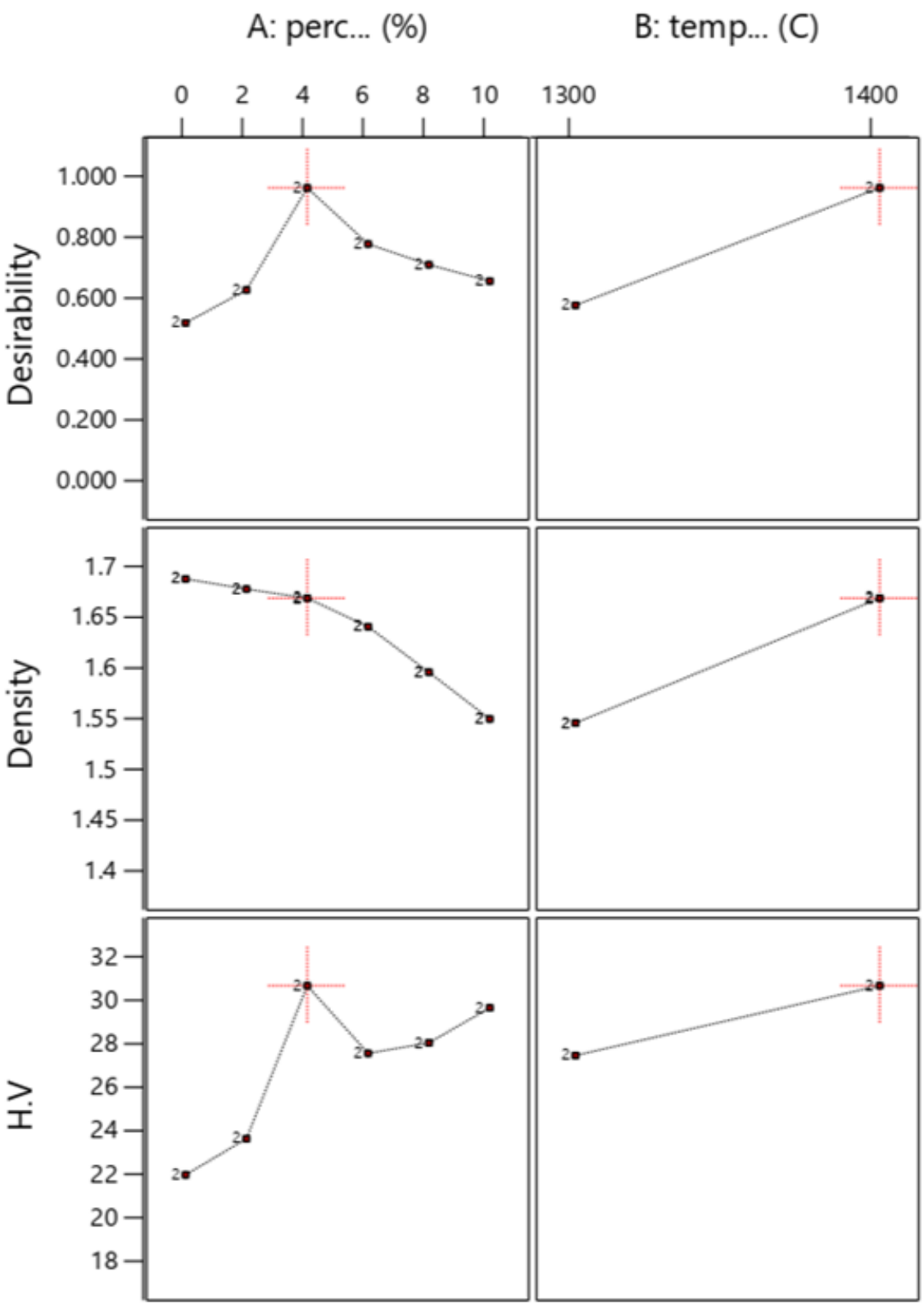

Figure (5.19) Response for individual factors

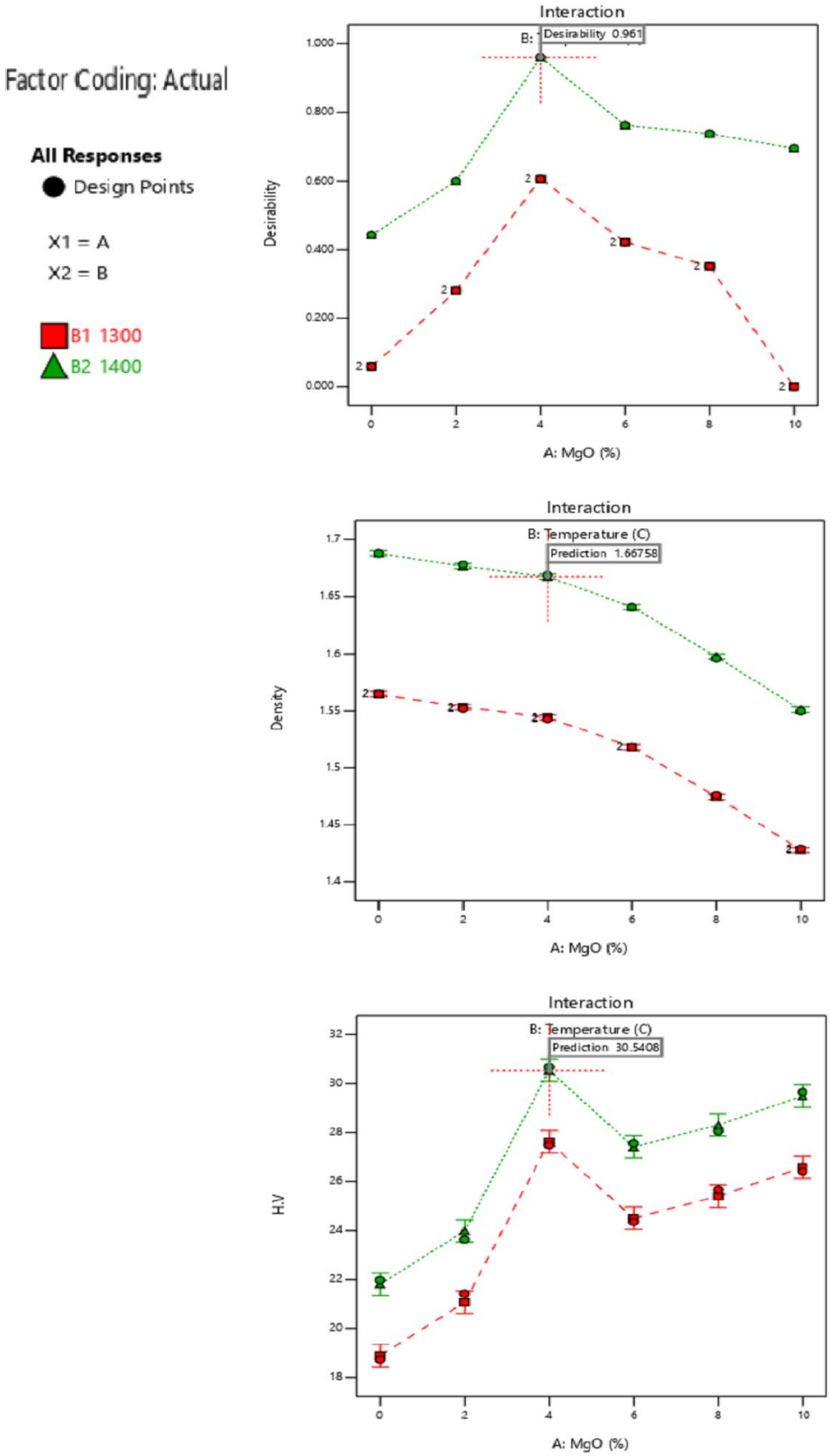

Figure (5.20) Response for all interaction of factors

Chapter Six

Conclusions & Recommendations

6.1 Conclusions

According to the results of the experimental work and optimization method, it can be concluded:

1. Alumina can be toughened with MgO -by refining the resulted grains, which improve the physical and the mechanical properties - but with ratio less than 4wt.% -to avoid an excess amount of spinal products.
2. Critical loads of Al_2O_3 with (0, 2, 4, 6, 8, 10 wt.) MgO were (7, 9, 12, 6, 7, 8) N, respectively.
3. KIC of Al_2O_3 with (0, 2, 4, 6, 8, 10 wt.) MgO were (0.713, 0.857, 1.264, 0.648, 0.699, 0.831) ($MPa.m^{-1}$), respectively.
4. DIC is appropriate technique to describe crack behavior (initiation and propagation of crack) for tested specimens that explain the localized deformation at all tested area.
5. Computerized Optimization Programs have a benefit to experimental design and resolve the complicated experiments with less time and cost.

6.2 Recommendations

1. Sintering the samples at higher temperature and deferent heating cycle.
2. Investigate the wear strength and compressive strength of the products.
3. Studying KIC of the product's specimens by using an indentation technique.
4. Make more investigations on the microstructure for fracture's surface to get more information about the effect of Magnesia on the Alumina.
5. Investigation 3D crack of Alumina with digital image correlation.
6. Making more specimens with deferent conditions to get a more precise results by using "Design Expert" optimization program.

References

[1] A. Arab, Z. D. I. Sktani, Q. Zhou, Z. A. Ahmad, and P. Chen, "Effect of MgO addition on the mechanical and dynamic properties of zirconia toughened alumina (ZTA) ceramics," *Materials*, vol. 12, no. 15. 2019. doi: 10.3390/ma12152440.

[2] P. Milak, F. D. Minatto, C. Faller, A. De Noni, and O. R. Klegues Montedo, "The influence of dopants in the grain size of alumina - A review," in *Materials Science Forum*, 2015, vol. 820, pp. 280–284. doi: 10.4028/www.scientific.net/MSF.820.280.

[3] Z. Harun, N. F. Ismail, and N. A. Badarulzaman, "Effect of MgO additive on microstructure of Al_2O_3," *Advanced Materials Research*, vol. 488–489. pp. 335–339, 2012. doi: 10.4028/www.scientific.net/AMR.488-489.335.

[4] L. C. S. Nunes and J. M. L. Reis, "Estimation of crack-tip-opening displacement and crack extension of glass fiber reinforced polymer mortars using digital image correlation method," *Materials and Design*, vol. 33, no. 1. pp. 248–253, 2012. doi: 10.1016/j.matdes.2011.07.051.

[5] J. J. Mecholsky, "Fracture mechanics principles," *Dental Materials*, vol. 11, no. 2. pp. 111–112, 1995. doi: 10.1016/0109-5641(95)80044-1.

[6] Z. X. Lin, Z. H. Xu, Y. H. An, and X. Li, "In situ observation of fracture behavior of canine cortical bone under bending," *Mater. Sci. Eng. C*, vol. 62, pp. 361–367, 2016, doi: 10.1016/j.msec.2016.01.061.

[7] W. Mekky and P. S. Nicholson, "The fracture toughness of Ni/Al_2O_3 laminates by digital image correlation I: Experimental crack opening displacement and R-curves," *Engineering Fracture Mechanics*, vol. 73,

no. 5. pp. 571–582, 2006. doi: 10.1016/j.engfracmech.2005.09.005.

[8] T. Brynk, A. Laptiev, O. Tolochyn, and Z. Pakiela, "Digital image correlation based method of crack growth rate and fracture toughness measurements on mini-samples," *Key Engineering Materials*, vol. 586. pp. 96–99, 2014. doi: 10.4028/www.scientific.net/KEM.586.96.

[9] M. Dadkhah, A. Saboori, and M. Jafari, "Investigating the Physical Properties of Sintered Alumina in the Presence of MgO Nanopowder," *Journal of Materials*, vol. 2014. pp. 1–7, 2014. doi: 10.1155/2014/496146.

[10] J. F. Shackelford and R. H. Doremus, "Ceramic and Glass Materials," *Ceramic and Glass Materials*. 2008. doi: 10.1007/978-0-387-73362-3.

[11] C. Piconi and A. A. Porporati, "Bioinert ceramics: Zirconia and alumina," *Handbook of Bioceramics and Biocomposites*. pp. 59–89, 2016. doi: 10.1007/978-3-319-12460-5_4.

[12] R. P. Singh and S. Singhal, "Investigation of machining characteristics in rotary ultrasonic machining of alumina ceramic," *Mater. Manuf. Process.*, vol. 32, no. 3, pp. 309–326, 2017, doi: 10.1080/10426914.2016.1176190.

[13] M. A. Shand, "The Chemistry and Technology of Magnesia," *The Chemistry and Technology of Magnesia*. pp. 1–266, 2006. doi: 10.1002/0471980579.

[14] M. Rahaman, *Ceramic Processing*. Taylor & Francis, 2007.

[15] M. N. Rahaman, *Ceramic processing*. Taylor & Francis Group, 2017. doi: 10.1201/9781315276045.

[16] R. Lecomber, C. Duprez, and E. S. Kirschen, "Handbook of Advanced

Ceramics," *The Economic Journal*, vol. 81, no. 322. p. 385, 1971. doi: 10.2307/2230089.

[17] W. D. Kingery, H. K. Bowen, and D. R. Uhlmann, "Introduction to ceramics (2nd edition)," *John Wiley & Sons, Inc.* p. 864, 1976.

[18] H. Erkalfa, Z. Misirli, M. Demirci, Ç. Toy, and T. Baykara, "The densification and microstructural development of Al_2O_3 with manganese oxide addition," *Journal of the European Ceramic Society*, vol. 15, no. 2. pp. 165–171, 1995. doi: 10.1016/0955-2219(95)93062-8.

[19] Y. K. Jeong and K. Niihara, "Microstructure and properties of alumina-silicon carbide nanocomposites fabricated by pressureless sintering and post hot-isostatic pressing," *Transactions of Nonferrous Metals Society of China (English Edition)*, vol. 21, no. SUPPL. 1. 2011. doi: 10.1016/S1003-6326(11)61050-9.

[20] R. W. Rice, *Ceramic Fabrication Technology*. Marcel Dekker, Inc., 2003.

[21] M. Sathiyakumar and F. D. Gnanam, "Influence of additives on density, microstructure and mechanical properties of alumina," *Journal of Materials Processing Technology*, vol. 133, no. 3. pp. 282–286, 2003. doi: 10.1016/S0924-0136(02)00956-1.

[22] Z. Zhihui, L. Nan, and R. Guozhi, "Effect of polymorphism of Al_2O_3 on sintering and grain growth of magnesia aluminate spinel," *Science of Sintering*, vol. 39, no. 1. pp. 9–15, 2007. doi: 10.2298/SOS0701009Z.

[23] M. A. L. Braulio, M. Rigaud, A. Buhr, C. Parr, and V. C. Pandolfelli, "Spinel-containing alumina-based refractory castables," *Ceramics International*, vol. 37, no. 6. pp. 1705–1724, 2011. doi: 10.1016/j.ceramint.2011.03.049.

[24] B. R. Lawn, T. R. Wilshaw, and J. R. Rice, “Fracture of Brittle Solids (Cambridge Solid State Science Series),” *Journal of Applied Mechanics*, vol. 44, no. 3. pp. 517–517, 1977. doi: 10.1115/1.3424125.

[25] B. Basu and K. Balani, “Advanced Structural Applications.” p. 502, 2011.

[26] G. E. Dieter, “Mechanical metallurgy.” McGRAW-HILL BOOK COMPANY, p. 646, 1961.

[27] M. S. Kaliszewski *et al.*, “Indentation Studies on Y_2O_2-Stabilized ZrO_2: I, Development of Indentation-Induced Cracks,” *Journal of the American Ceramic Society*, vol. 77, no. 5. pp. 1185–1193, 1994. doi: 10.1111/j.1151-2916.1994.tb05391.x.

[28] G. D. Quinn and R. C. Bradt, “On the vickers indentation fracture toughness Test,” *Journal of the American Ceramic Society*, vol. 90, no. 3. pp. 673–680, 2007. doi: 10.1111/j.1551-2916.2006.01482.x.

[29] B. R. Lawn, “Indentation of ceramics with spheres: A century after Hertz,” *Journal of the American Ceramic Society*, vol. 81, no. 8. pp. 1977–1994, 1998. doi: 10.1111/j.1151-2916.1998.tb02580.x.

[30] A. Bakker, “Elastic-plastic fracture mechanics analysis of an SENB specimen,” *International Journal of Pressure Vessels and Piping*, vol. 10, no. 6. pp. 431–449, 1982. doi: 10.1016/0308-0161(82)90004-7.

[31] B. S. Li, T. J. Marrow, S. G. Roberts, and D. E. J. Armstrong, “Evaluation of Fracture Toughness Measurements Using Chevron-Notched Silicon and Tungsten Microcantilevers,” *Jom*, vol. 71, no. 10. pp. 3378–3389, 2019. doi: 10.1007/s11837-019-03696-1.

[32] H. Tada, P. C. Paris, and G. R. Irwin, "Stress Analysis Results for Common Test Specimen Configurations," *The Stress Analysis of Cracks Handbook, Third Edition*. pp. 39–80, 2010. doi: 10.1115/1.801535.ch2.

[33] ASTM International, "Astm C1421-10," *Standard Test Methods for Determination of Fracture Toughness of Advanced Ceramics at Ambient Temperature*. pp. 20–23, 2014. [Online]. Available: www.astm.org,

[34] B. Basu, J. Vleugels, and O. Van Der Biest, "Microstructure-toughness-wear relationship of tetragonal zirconia ceramics," *Journal of the European Ceramic Society*, vol. 24, no. 7. pp. 2031–2040, 2004. doi: 10.1016/S0955-2219(03)00355-8.

[35] P. CHANTIKUL, G. R. ANSTIS, B. R. LAWN, and D. B. MARSHALL, "A Critical Evaluation of Indentation Techniques for Measuring Fracture Toughness: II, Strength Method," *Journal of the American Ceramic Society*, vol. 64, no. 9. pp. 539–543, 1981. doi: 10.1111/j.1151-2916.1981.tb10321.x.

[36] R. Korobkint, C. Guthrie, B. Macleod, and J. Rachlinski, "Bounded Rationality , Standard Form Contracts , and Unconscionability and the University of Nevada-Las Vegas Boyd School of Law ; as well as from Jennifer Arlen ," *University of Chicago Law Review*, vol. 70, no. 4. pp. 1203–1295, 2010.

[37] J. E. P. IPINA, "CTOD for slow stable crack growth conditions," *Fatigue Eng. Mater. Ltd*, vol. 15, no. 11, pp. 1091–1100, 1992.

[38] M. F. Kanninen and C. H. Popelar, "Advanced fracture mechanics," *International Journal of Fracture*, vol. 30, no. 4. International Journal of

Fracture, pp. R73–R74, 1986. doi: 10.1007/bf00019713.

[39] N. O'Dowd, "Advanced Fracture Mechanics: Lectures On Fundamentals Of Elastic, Elastic-Plastic And Creep Fracture," *Journal of Engineering Materials and Technology*. p. 107, 2002.

[40] M. Demetriou, G. Garrett, M. E Launey, and J. P Schramm, "A damage-tolerant glass." ResearchGate, p. 10, 2011. doi: 10.1038/nmat2930.

[41] F. Mathieu, F. Hild, and S. Roux, "Identification of a crack propagation law by digital image correlation," *International Journal of Fatigue*, vol. 36, no. 1. pp. 146–154, 2012. doi: 10.1016/j.ijfatigue.2011.08.004.

[42] S. Roux, J. Réthoré, and F. Hild, "Digital image correlation and fracture: An advanced technique for estimating stress intensity factors of 2D and 3D cracks," *Journal of Physics D: Applied Physics*, vol. 42, no. 21. 2009. doi: 10.1088/0022-3727/42/21/214004.

[43] I. S. Koltsida, A. K. Tomor, and C. A. Booth, "the Use of Digital Image Correlation Technique for Monitoring Masonry Arch," *7th International Conference on Arch Bridges*, no. October 2013. pp. 681–690, 2013.

[44] P. F. Luo, Y. J. Chao, M. A. Sutton, and W. H. Peters, "Accurate measurement of three-dimensional deformations in deformable and rigid bodies using computer vision," *Experimental Mechanics*, vol. 33, no. 2. pp. 123–132, 1993. doi: 10.1007/BF02322488.

[45] G. Cai, L. Liang, X. Zhao, and R. Zheng, "Patterns support for automatic service composition," *IEEE International Conference on Automation and Logistics, ICAL*. pp. 101–104, 2012. doi: 10.1109/ICAL.2012.6308178.

[46] B. Pan, K. Qian, H. Xie, and A. Asundi, "2D DIC for in-plane displacement and strain measurement : a review," *Measurement Science and Technology*, vol. 20. pp. 1–17, 2009.

[47] Q. Lin and J. F. Labuz, "Fracture of sandstone characterized by digital image correlation," *International Journal of Rock Mechanics and Mining Sciences*, vol. 60. pp. 235–245, 2013. doi: 10.1016/j.ijrmms.2012.12.043.

[48] J. Pittari and G. Subhash, "Fracture Toughness Testing of Advanced Silicon Carbide Ceramics Using Digital Image Correlation," *Conference Proceedings of the Society for Experimental Mechanics Series*, vol. 65, no. VOLUME 1. pp. 207–212, 2015. doi: 10.1007/978-3-319-06995-1_31.

[49] M. M. H. Albo-Jasim, M. A. Aswad, and H. K. Rashed, "Investigation of crack propagation and opening in hydroxyapatite using digital image correlation," *J. Eng. Appl. Sci.*, vol. 12, no. Specialissue6, pp. 7935–7943, 2017, doi: 10.3923/jeasci.2017.7935.7943.

[50] M. A. Aswad, I. K. Sabree, and A. H S Abd, "An examination of the effect of adding zirconia to bioactive glass-ceramic properties," *IOP Conference Series: Materials Science and Engineering*, vol. 1067, no. 1. p. 012121, 2021. doi: 10.1088/1757-899x/1067/1/012121.

[51] M. I. Oribi, "Optimization of PSZ Addition Upon Fracture Mechanics of Hydroxyapatite Using Digital Image Correlation," University of Babylon, 2022.

[52] S. R. Rao and G. Padmanabhan, "Application of Taguchi methods and ANOVA in optimization of process parameters for metal removal rate in electrochemical machining of Al/5% SiC composites," *International*

Journal of Engineering Research and …, vol. 2, no. 3. pp. 192–197, 2012.

[53] J. A. Wass, "Design-Expert 7.0," *Biotech Software & Internet Report*, vol. 2, no. 2. pp. 71–73, 2001. doi: 10.1089/152791601750193733.

[54] I. Sopyan and S. Sriwidodo, "DESIGN-EXPERT SOFTWARE (DOE). AN APPLICATION TOOL FOR OPTIMIZATION IN PHARMACEUTICAL PREPARATIONS FORMULATION." International Journal of Applied Pharmaceutics, p. 9, 2022. doi: 10.22159/ijap.2022v14i4.45144.

[55] S. Bolton and C. Bon, *Pharmaceutical Statistics*. New York: Informa Healthcare USA, 2010.

[56] ASTM, "Standard Test Methods for Apparent Porosity, Water Absorption, Apparent Specific Gravity, and Bulk Density of Burned Refractory Brick and Shapes by Boiling Water 1 This international standard was developed in accordance with internationally recognized pri," *ASTM International*, vol. 00, no. Reapproved 2015. pp. 20–22, 2022.

[57] ASTM D2845-08, "Determination of Pulse Velocities and Ultrasonic Elastic Constants of Rock," *Designation: D 2845 – 00*, vol. 14, no. April 1996. pp. 1–9, 2017. [Online]. Available: https://www.astm.org/

[58] ISO/ASTM International, "Designation: E384-17 Standard Test Method for Microindentation Hardness of Materials," *The Biology of the Xenarthra*. pp. 281–293, 2017.

[59] C. Y. Tan, S. Ramesh, R. Tolouei, I. Sopyan, and W. D. Teng, "Synthesis of high fracture toughness of hydroxyapatite bioceramics," *Advanced Materials Research*, vol. 264–265. pp. 1849–1855, 2011. doi:

10.4028/www.scientific.net/AMR.264-265.1849.

[60] M. Tiegel, R. Hosseinabadi, S. Kuhn, A. Herrmann, and C. Rüssel, "Young's modulus, Vickers hardness and indentation fracture toughness of alumino silicate glasses," *Ceramics International*, vol. 41, no. 6. pp. 7267–7275, 2015. doi: 10.1016/j.ceramint.2015.01.144.

[61] C. Y. Tan *et al.*, "Sintering and mechanical properties of MgO-doped nanocrystalline hydroxyapatite," *Ceramics International*, vol. 39, no. 8. pp. 8979–8983, 2013. doi: 10.1016/j.ceramint.2013.04.098.